Supplementary Information

Design of porous of self-assembled homoleptic and heterolepetic Pd^{2+} cages incorporating Silicon-based Fluoride Acceptors: the way towards nuclear imaging applications

Marike Drexler,[a] Ioannis Kanavos,[b] Daniela Krauss,[a] Guillermo Moreno-Alcántar,[a] Lydia M. Smith,[c] Madeleine E. George,[c] Timothy H. Witney,[c] Ryszard Lobinski,[b,d] Luisa Ronga,[b,*] Angela Casini[a,*]

[a]Chair of Medicinal and Bioinorganic Chemistry, TUM School of Natural Sciences, Technical University of Munich, Garching bei München, Germany

[b]Université de Pau et des Pays de l'Adour, E2S UPPA, CNRS, IPREM, Pau, France. 2 Av. du Président Pierre Angot, Pau, France.

[c]School of Biomedical Engineering and Imaging Sciences, King's College London, St. Thomas' Hospital, London SE1 7EH London, United Kingdom.

[d]Chair of Analytical Chemistry, Warsaw University of Technology, ul. Noakowskiego 3, 00-664 Warszawa, Poland.

*** Correspondence:**
Angela Casini
angela.casini@tum.de

Luisa Ronga
luisa.ronga@univ-pau.fr

Table of Contents

1 Characterization of the ligands 3

1.1 2-(3,5-bis(pyridin-3-ylethynyl)phenyl)acetic acid (L0) 3

1.2 $_{D}$PepH3-$_{D}$Dap((SiFA)BA)-Ebes-L0 (L1) 7

1.3 $_{D}$PepH3-(SiFA)SeFe-Ebes-L0 (L2) 11

2 Homoleptic metallacages $C1_{hom}$ and $C2_{hom}$ 15

2.1 Characterization of $[Pd_2(L1)_4](BF_4)_4$ ($C1_{hom}$) 15

2.2 Characterization of $[Pd_2(L2)_4](BF_4)_4$ ($C2_{hom}$) 19

2.3 Stability of $C1_{hom}$ and $C2_{hom}$ in DMSO (1 mM) 22

2.4 Stability of $C1_{hom}$ and $C2_{hom}$ in different solvents (0.1 mM) 23

2.5 Concentration dependent formation of $C1_{hom}$ and $C2_{hom}$ 25

3 Heteroleptic metallacages $C1_{het}$ and $C2_{het}$ 26

3.1 Characterization of $C1_{het}$ 26

3.2 Characterization of $C2_{het}$ 31

4 Encapsulation of ReO_4^- 36

5 Characterization of radiolabeled ligands 37

5.1 ^{18}F-L1 37

5.2 ^{18}F-L2 38

6 Literature examples of Pd-based metallacages for imaging applications 39

1 Characterization of the ligands

1.1 2-(3,5-bis(pyridin-3-ylethynyl)phenyl)acetic acid (L0)

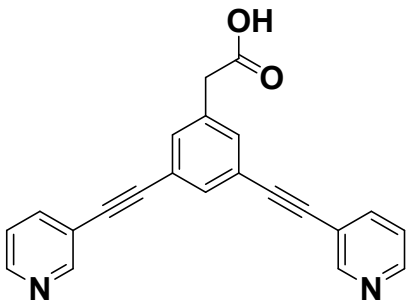

$C_{22}H_{14}N_2O_2$
338.37 g/mol

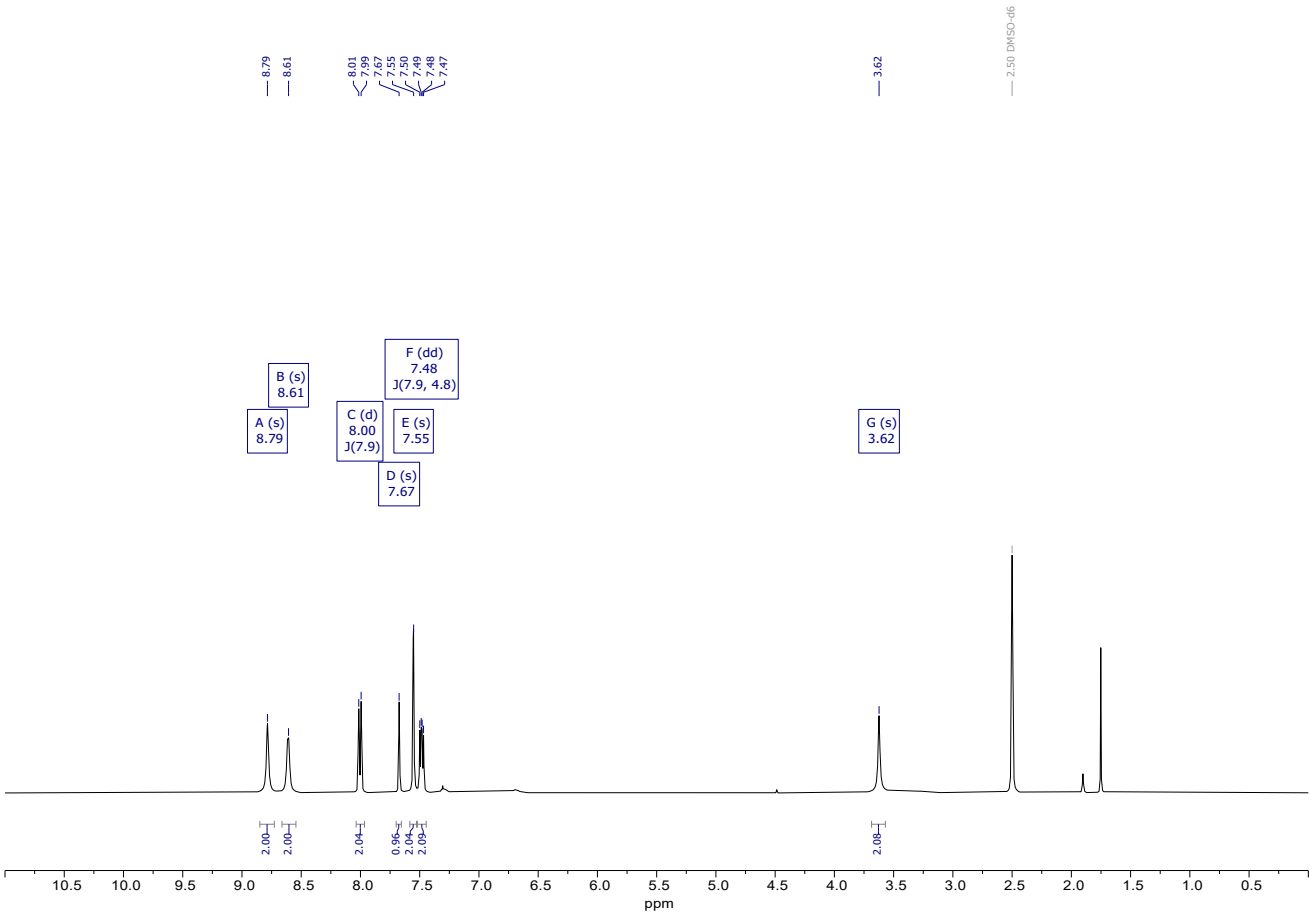

Figure S 1 - ^{1}H NMR spectrum of **L0** measured in DMSO-d_6 at 400 MHz.

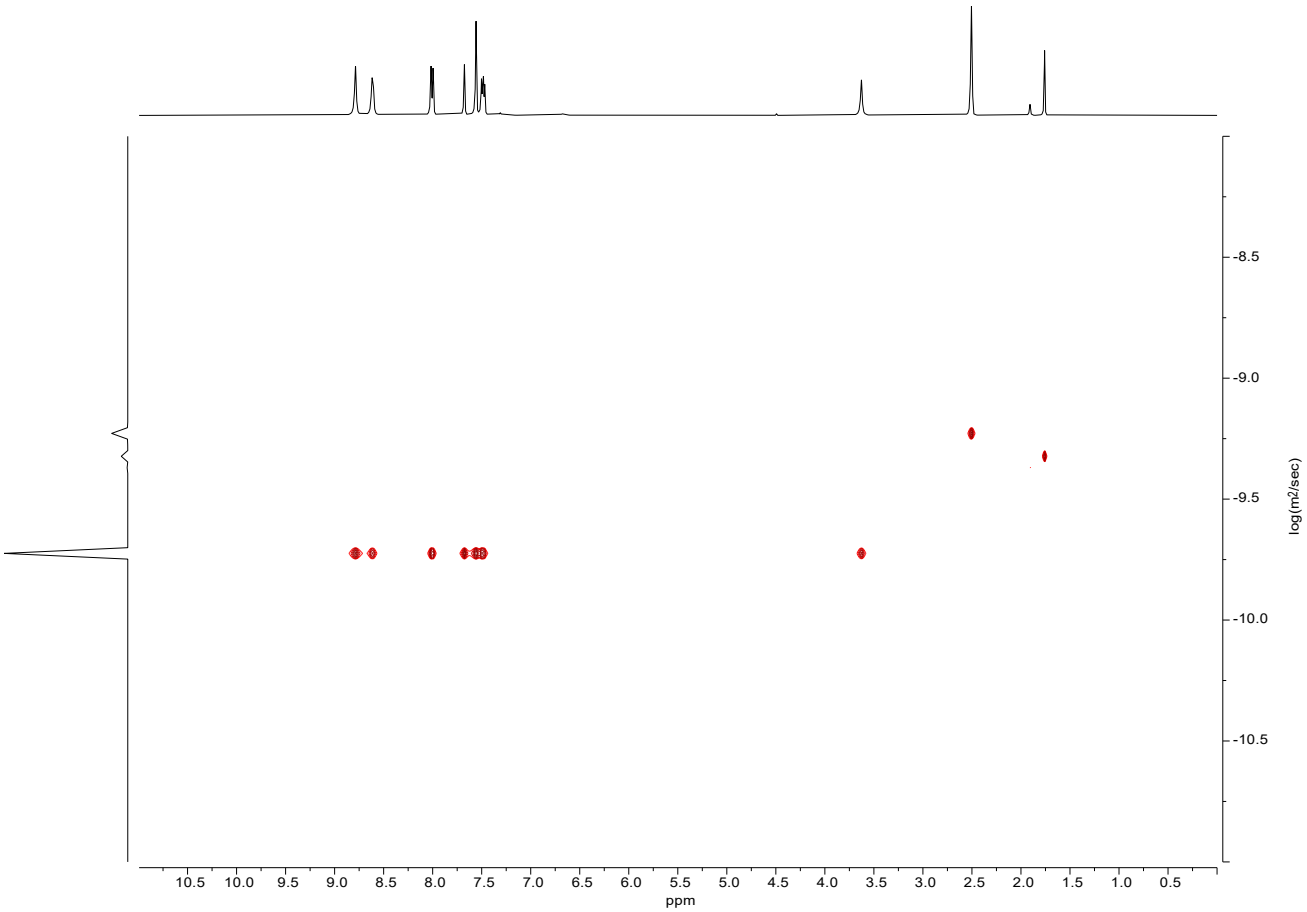

Figure S 2 - ^{1}H-DOSY NMR spectrum of **L0** measured in DMSO-d_6 at 400 MHz.

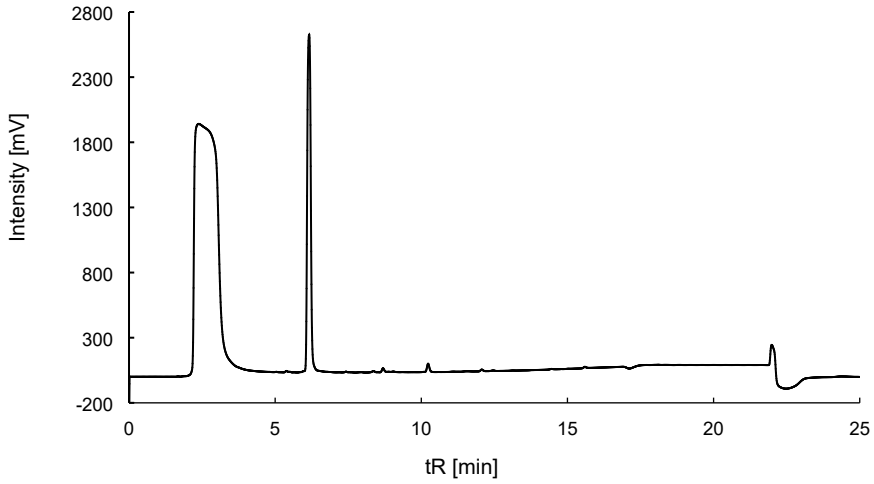

Figure S 3 - RP-HPLC chromatogram of **L0** measured with a gradient of 10-90% B in 15 min.

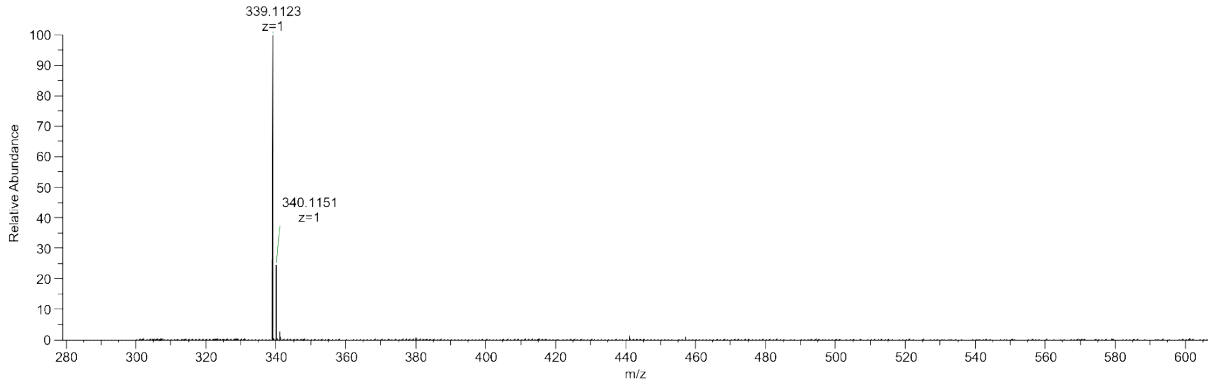

Figure S 4 - LC-HR-ESI-MS spectrum of **L0**. Mass spectrum at t_R= 8.38. The mobile phases were A: H_2O and B: ACN, both with 0.1% formic acid (FA). The flow rate used was 0.5 mL min^{-1} and sample elution was performed by using a gradient from 20% to 40% of B over 3 min, followed by a gradient from 40% to 80% of B over 15 min.

1.2 $_{D}$PepH3-$_{D}$Dap((SiFA)BA)-Ebes-L0 (L1)

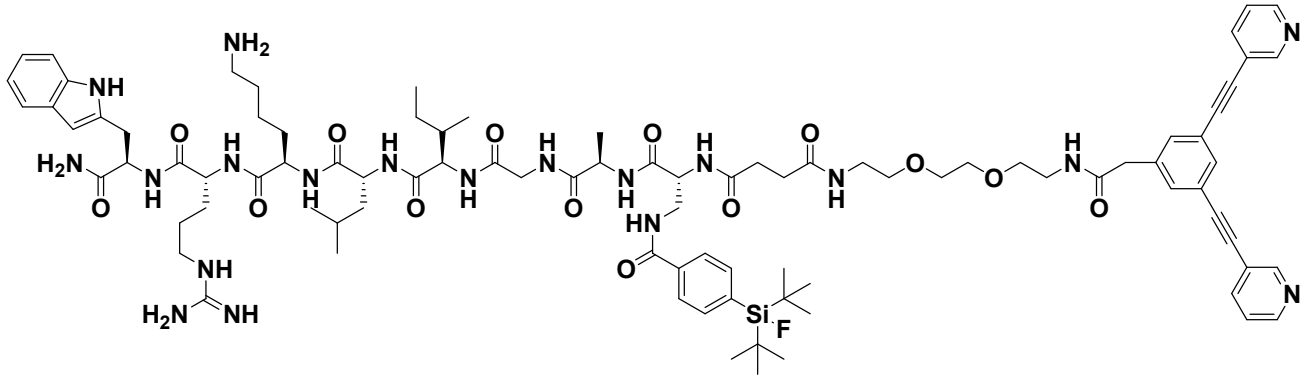

$C_{90}H_{124}FN_{19}O_{14}Si$
1743.18 g/mol

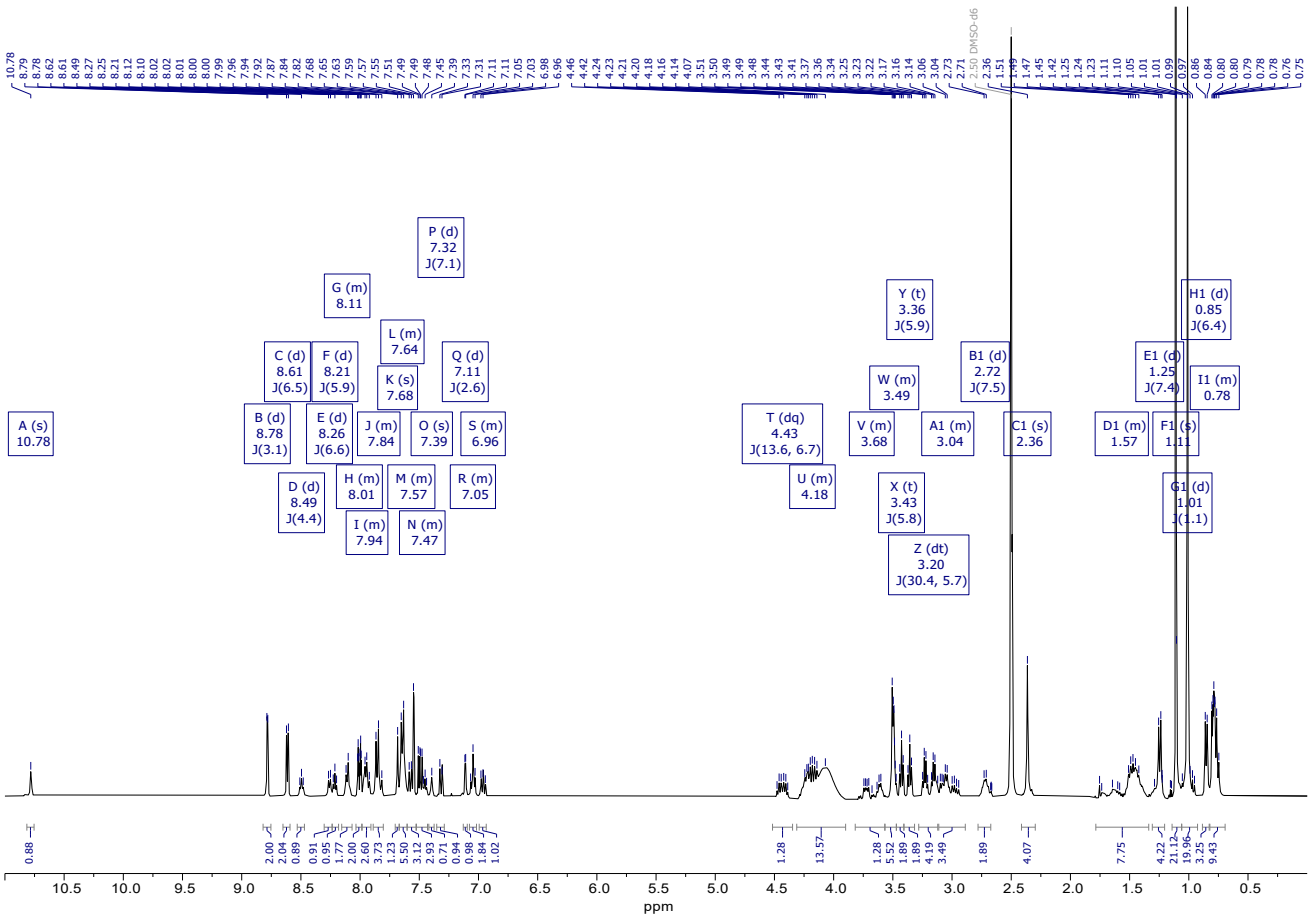

Figure S 5 - ^{1}H NMR spectrum of **L1** measured in DMSO-d_6 at 400 MHz.

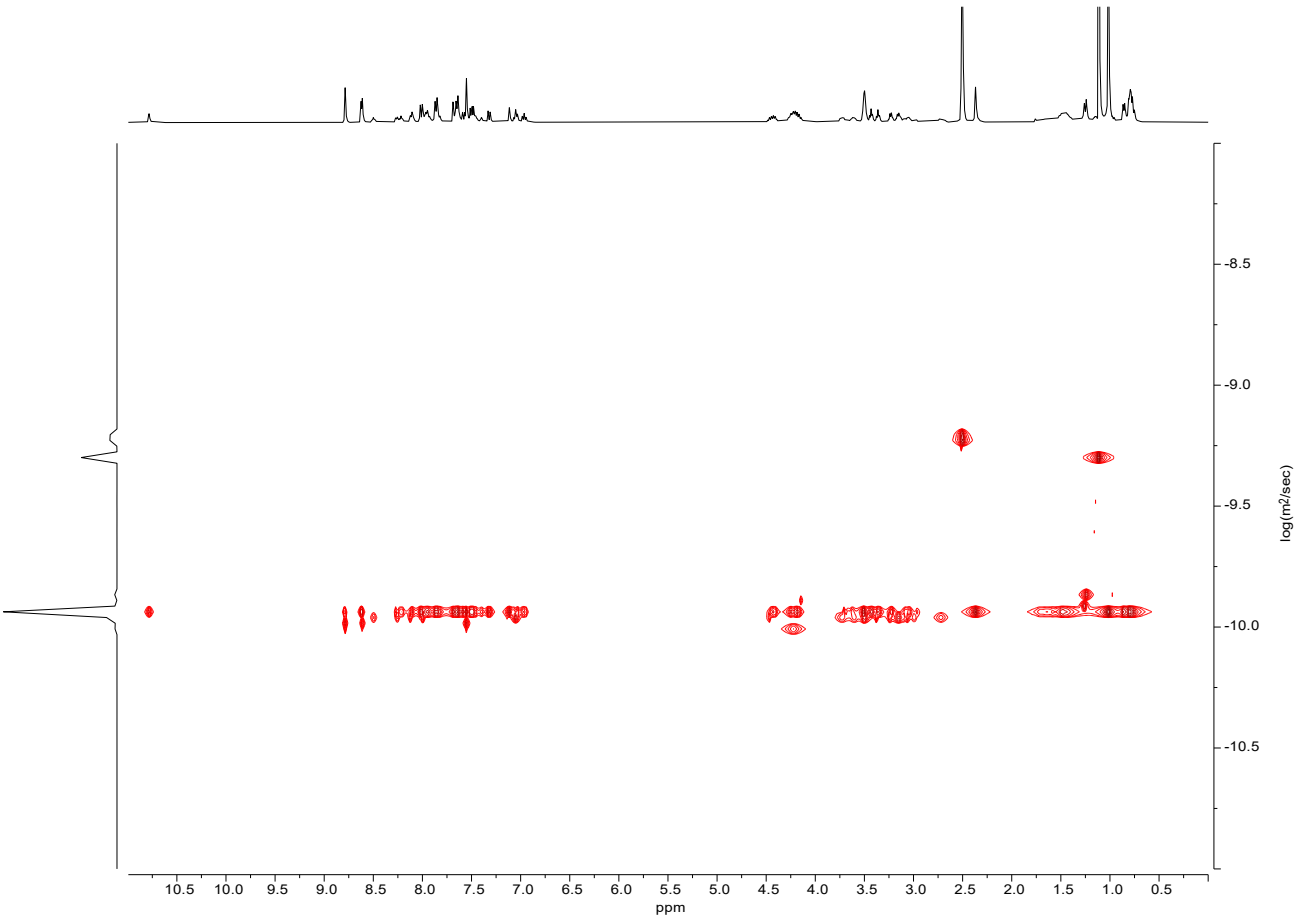

Figure S 6 - ^{1}H-DOSY NMR spectrum of **L1** measured in DMSO-d_6 at 400 MHz.

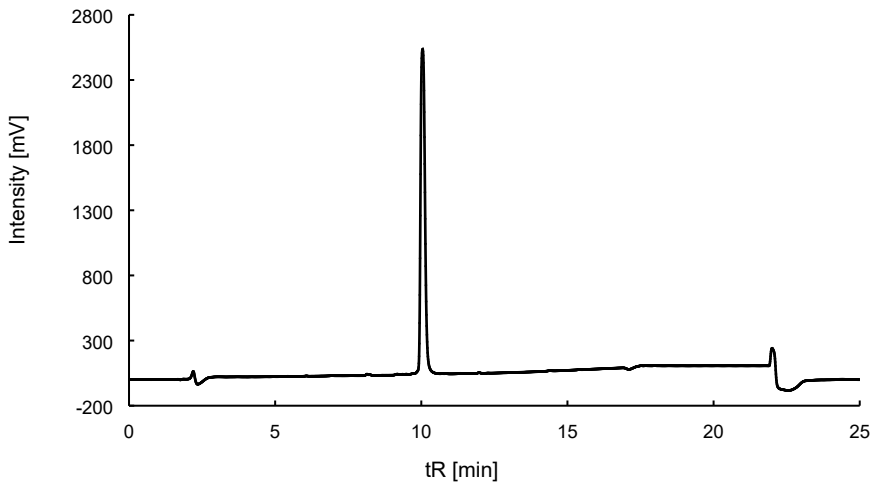

Figure S 7 - RP-HPLC chromatogram of **L1** measured with a gradient of 10-90% B in 15 min on a C18 column.

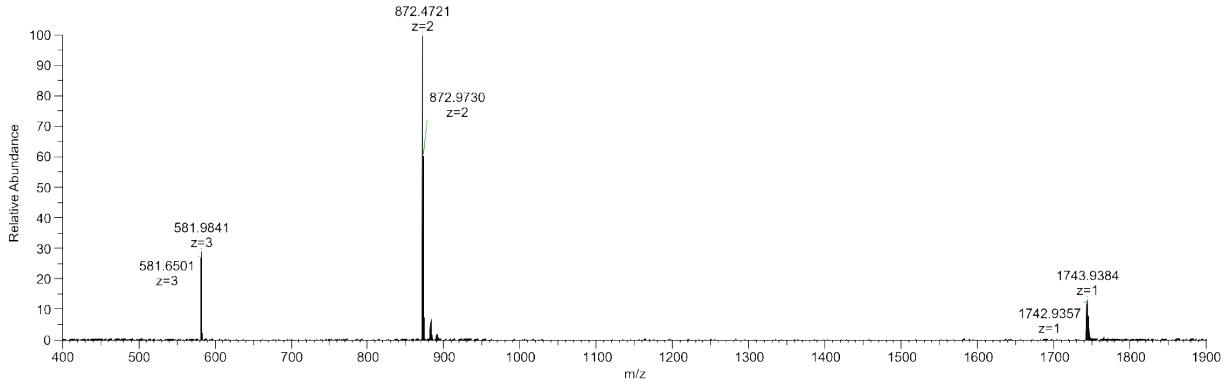

Figure S 8 - LC-HR-ESI-MS spectrum of **L1**. Mass spectrum at t_R= 9.30. The mobile phases were A: H_2O and B: ACN, both with 0.1% formic acid (FA). The flow rate used was 0.5 mL min^{-1} and sample elution was performed by using a gradient from 20% to 40% of B over 3 min, followed by a gradient from 40% to 80% of B over 15 min.

1.3 $_{D}$PepH3-(SiFA)SeFe-Ebes-L0 (L2)

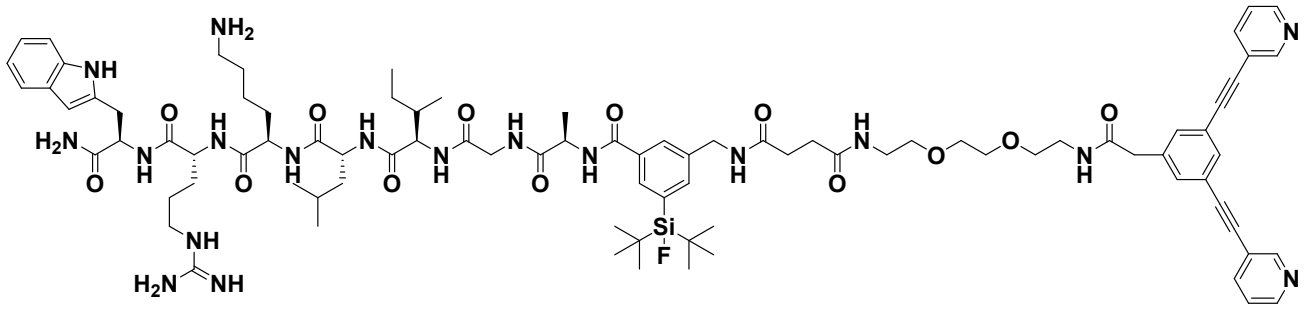

$C_{88}H_{121}FN_{18}O_{13}Si$
1686.13 g/mol

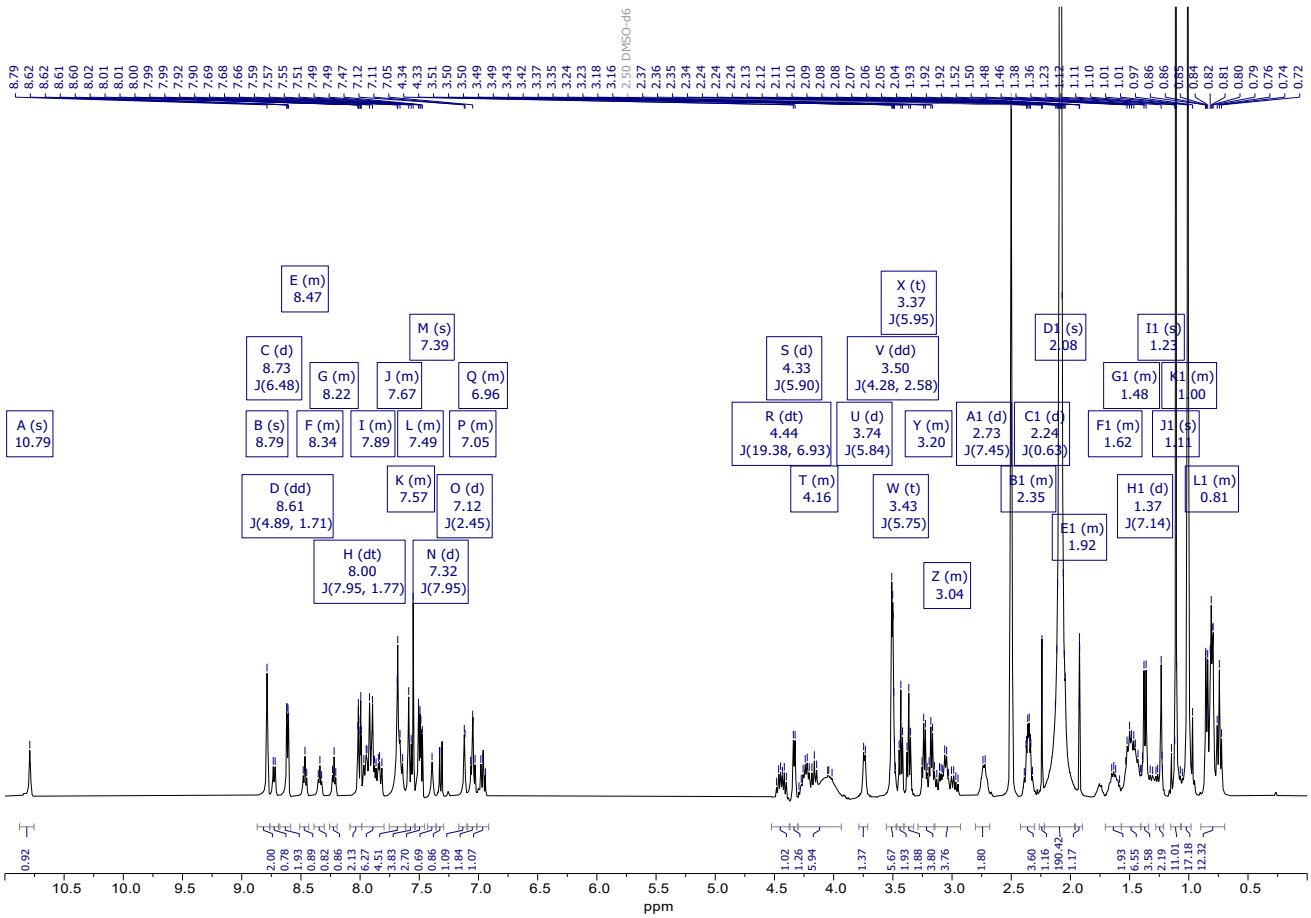

Figure S 9 - ^{1}H NMR spectrum of **L2** measured in DMSO-d_6 at 400 MHz.

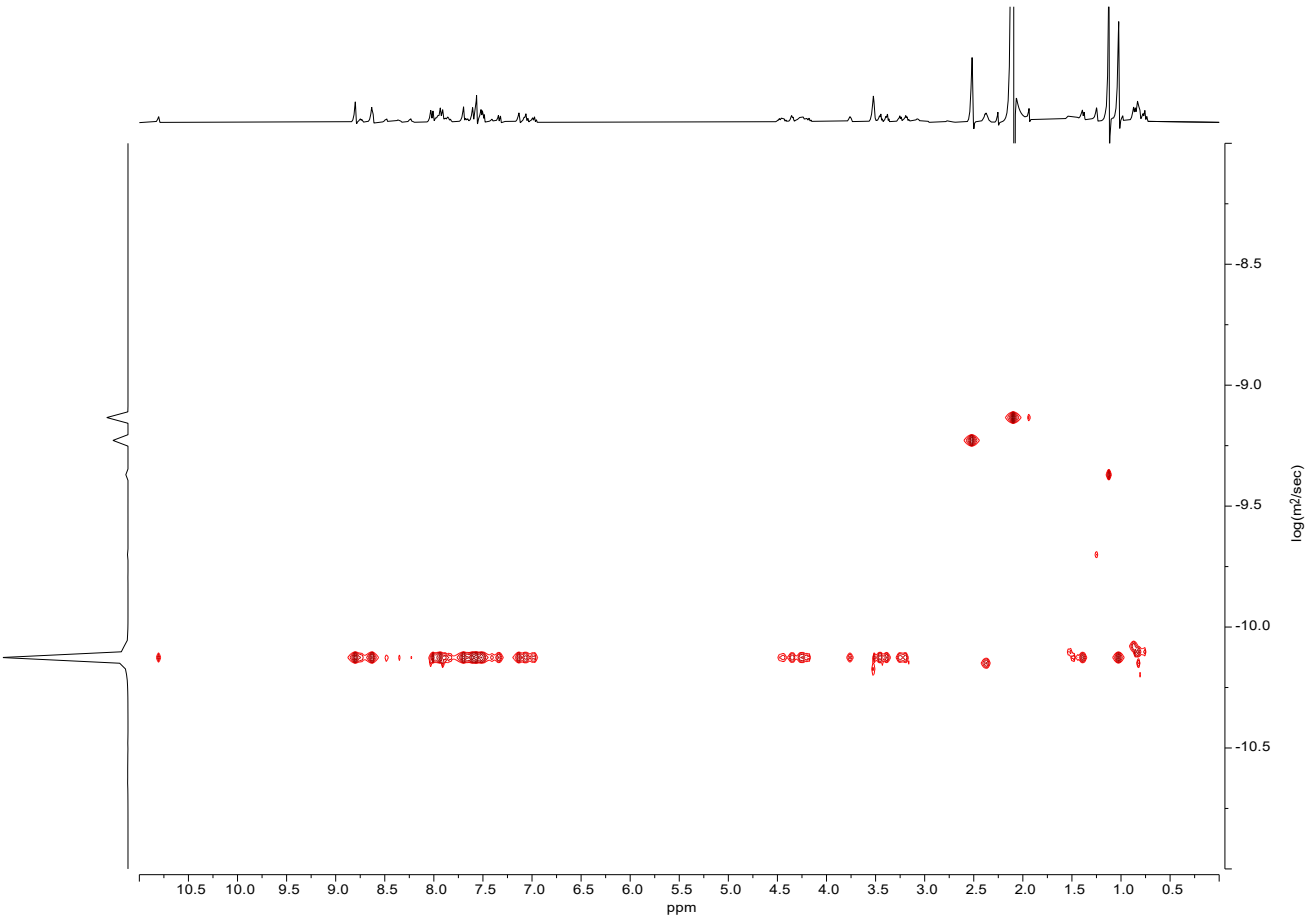

Figure S 10 - ^{1}H-DOSY NMR spectrum of **L2** measured in DMSO-d_6 at 400 MHz.

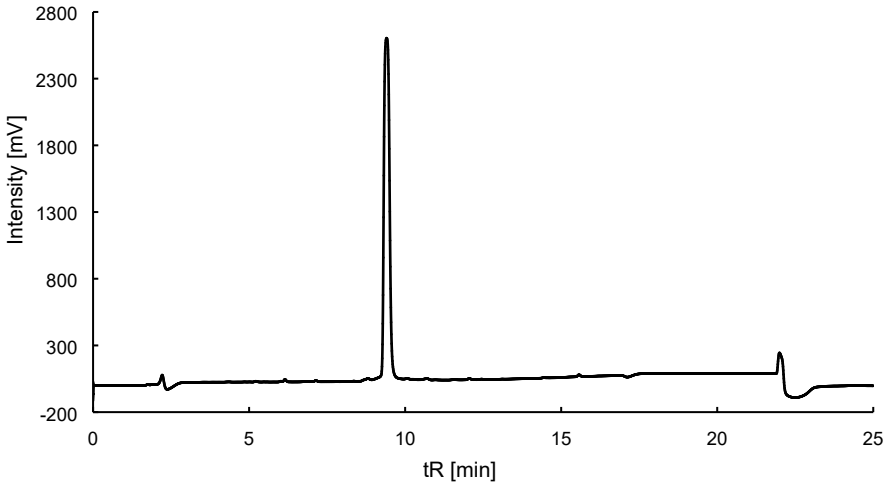

Figure S 11 - RP-HPLC chromatogram of **L2** measured with a gradient of 10-90% B in 15 min on a C18 column.

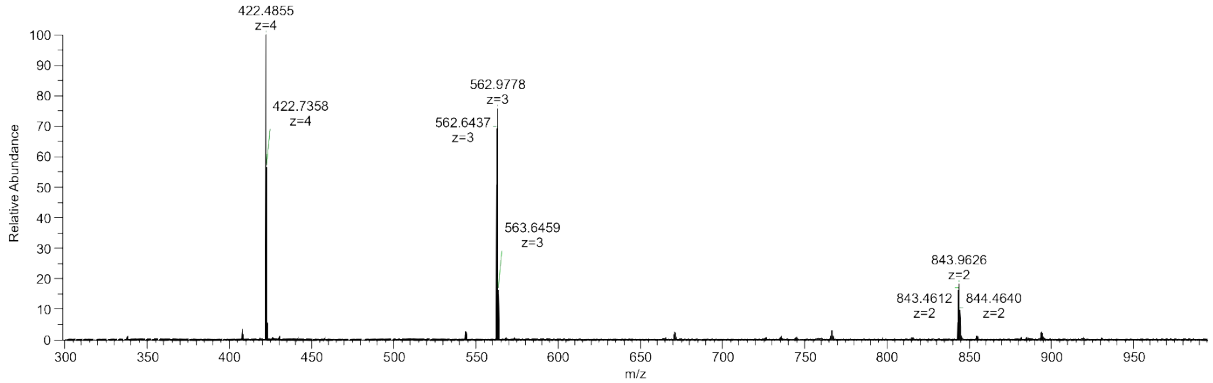

Figure S 12 - HR-ESI-MS spectrum of **L2**. Mass spectrum at t_R= 14.60. The mobile phases were A: H2O and B: MeCN, both with 0.1% formic acid (FA). The flow rate was 0.05 mL min-1 and sample elution was performed by using a gradient from 20% to 40% of B over 3 min, followed by a gradient from 40% to 80% of B over 15 min.

2 Homoleptic metallacages $C1_{hom}$ and $C2_{hom}$

2.1 Characterization of $[Pd_2(L1)_4](BF_4)_4$ ($C1_{hom}$)

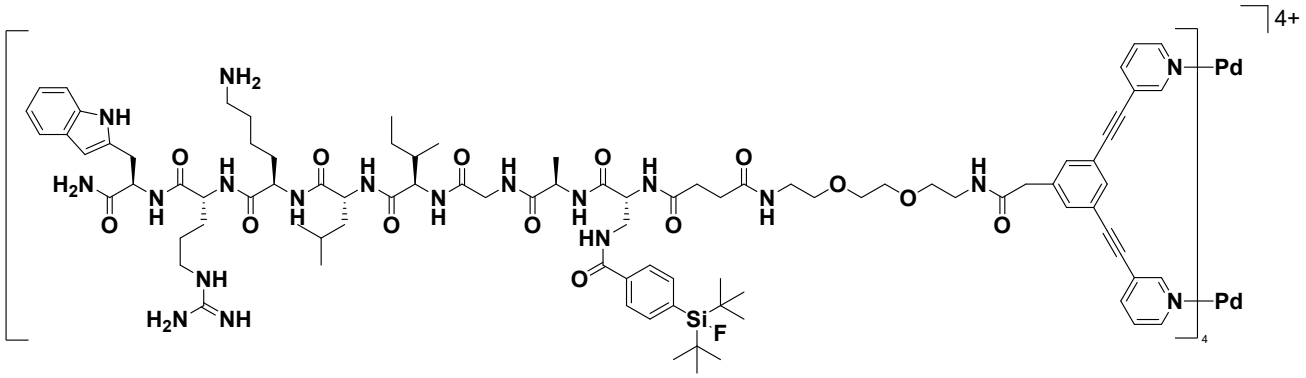

$C_{360}H_{496}F_4N_{76}O_{56}Pd_2Si_4^{4+}$
7185.58 g/mol

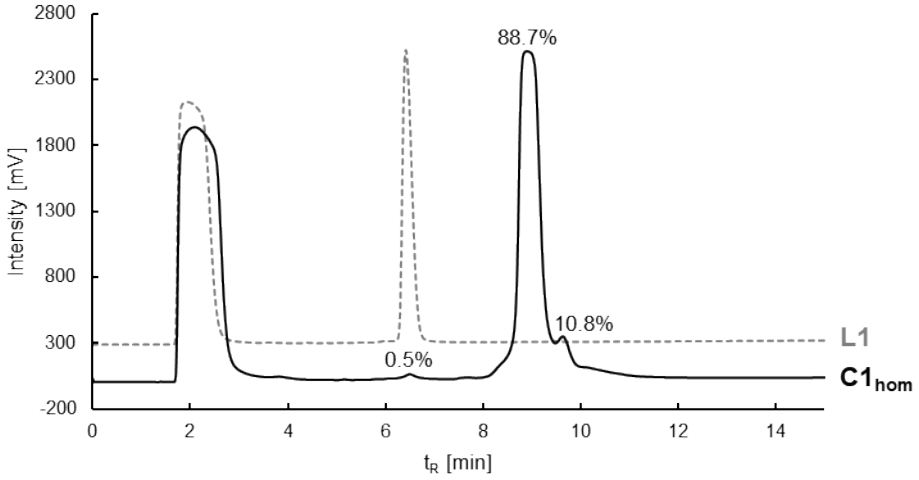

Figure S 13 - RP-HPLC chromatogram of **$C1_{hom}$** (1 mM) measured with a gradient of 40-70% B in 15 min. As a reference the chromatogram of the respective ligand **L1** is depicted in a grey dashed line.

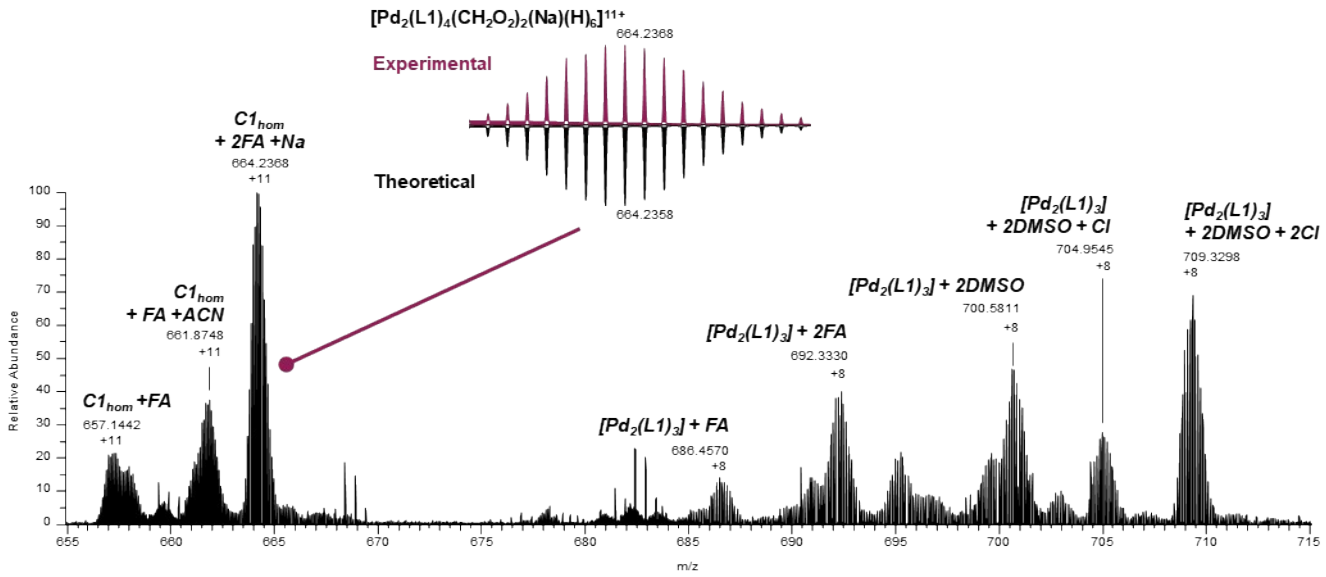

Figure S 14 - DI-HR-ESI-MS of **C1$_{hom}$**.

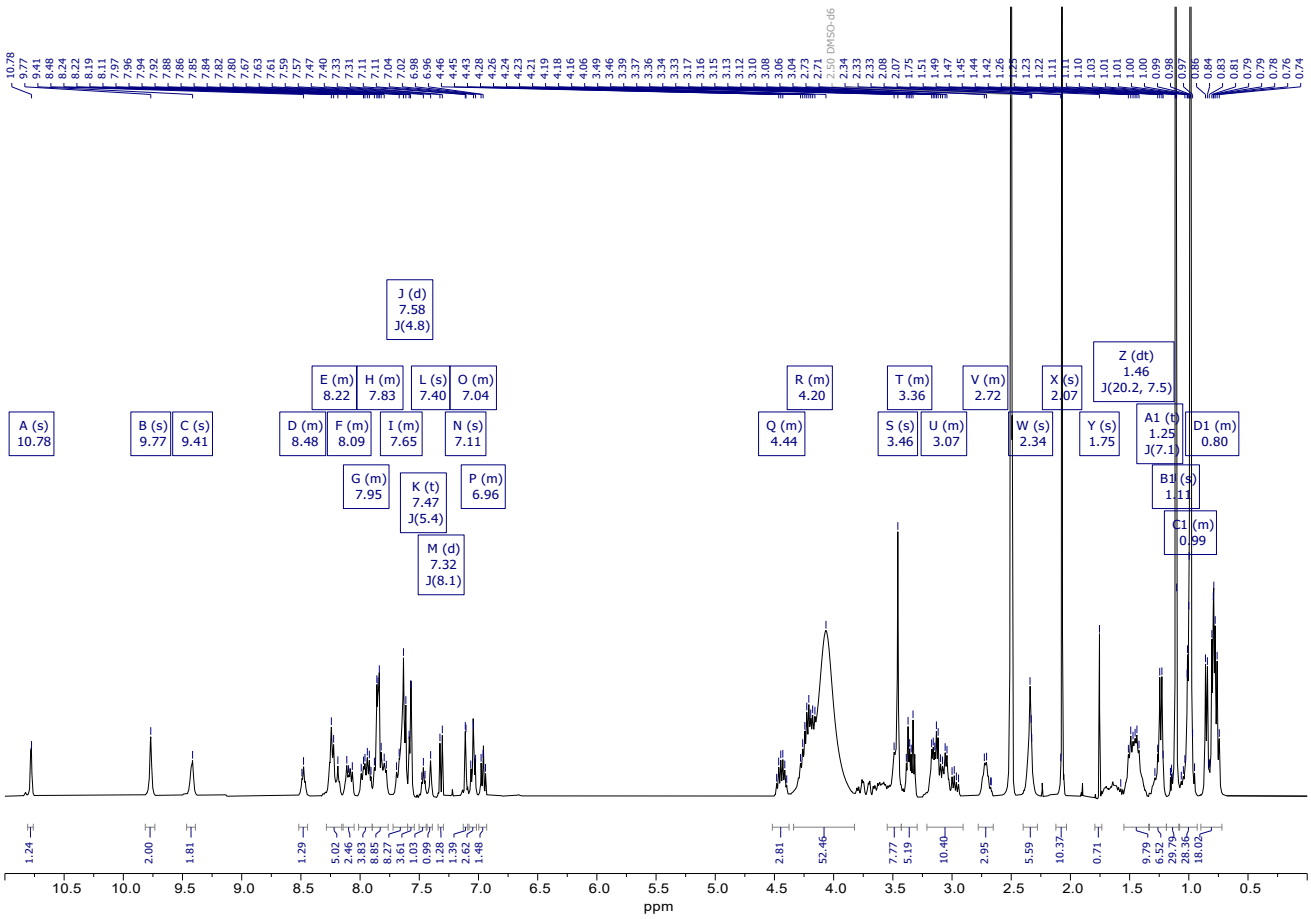

Figure S 15 - ^{1}H NMR spectrum of **C1$_{hom}$** measured in DMSO-d_6 at 400 MHz.

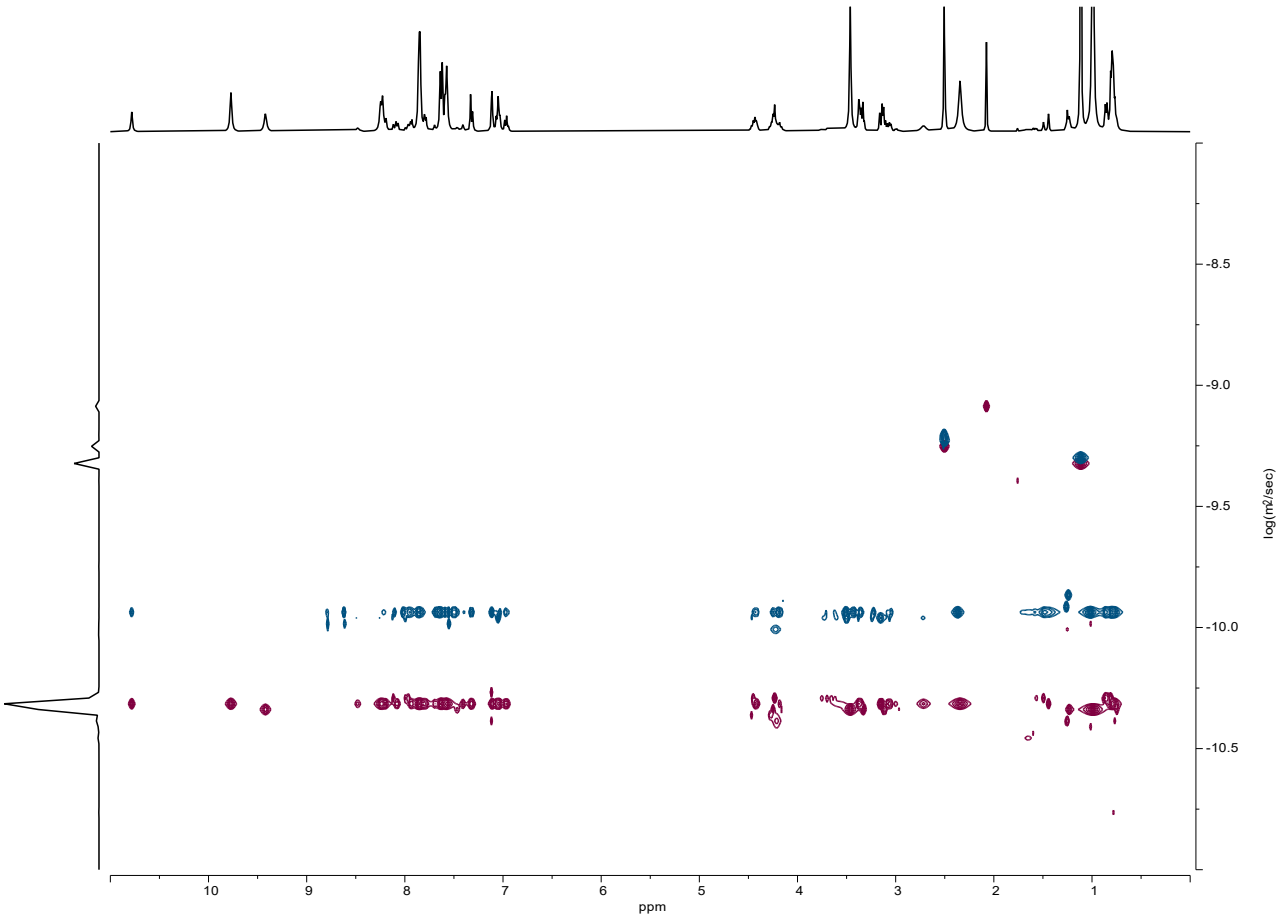

Figure S 16 - ^{1}H-DOSY NMR spectrum of **C1$_{hom}$** (purple) measured in DMSO-d_6 at 400 MHz. The ^{1}H-DOSY NMR spectrum of **L1** is shown in blue as a reference.

2.2 Characterization of $[Pd_2(L2)_4](BF_4)_4$ ($C2_{hom}$)

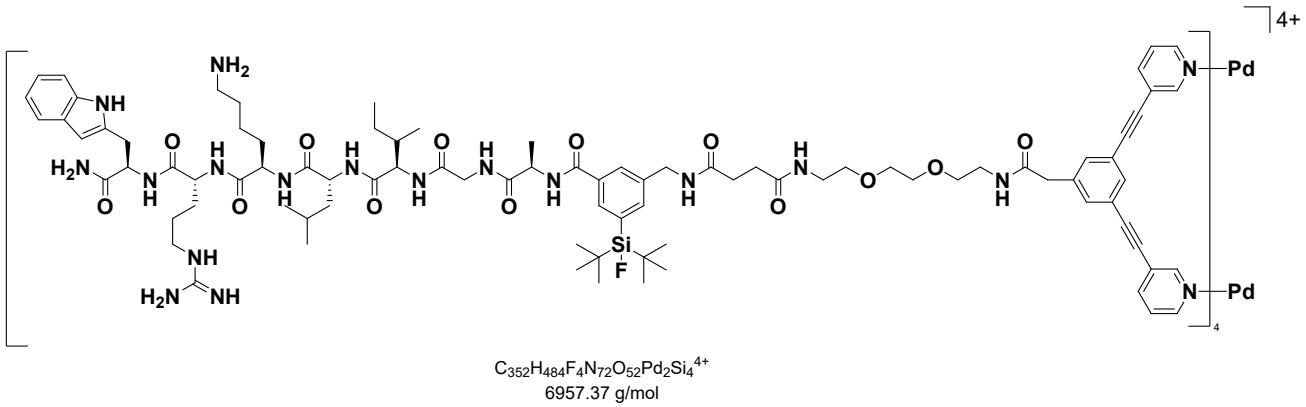

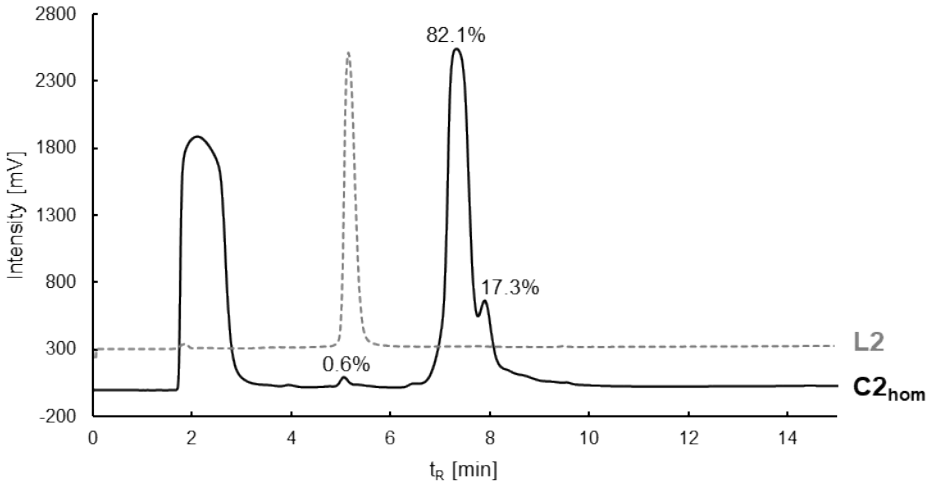

Figure S 17 - RP-HPLC chromatogram of **$C2_{hom}$** (1 mM) measured with a gradient of 40-70% B in 15 min. As a reference the chromatogram of the respective ligand **L2** is depicted in a grey dashed line.

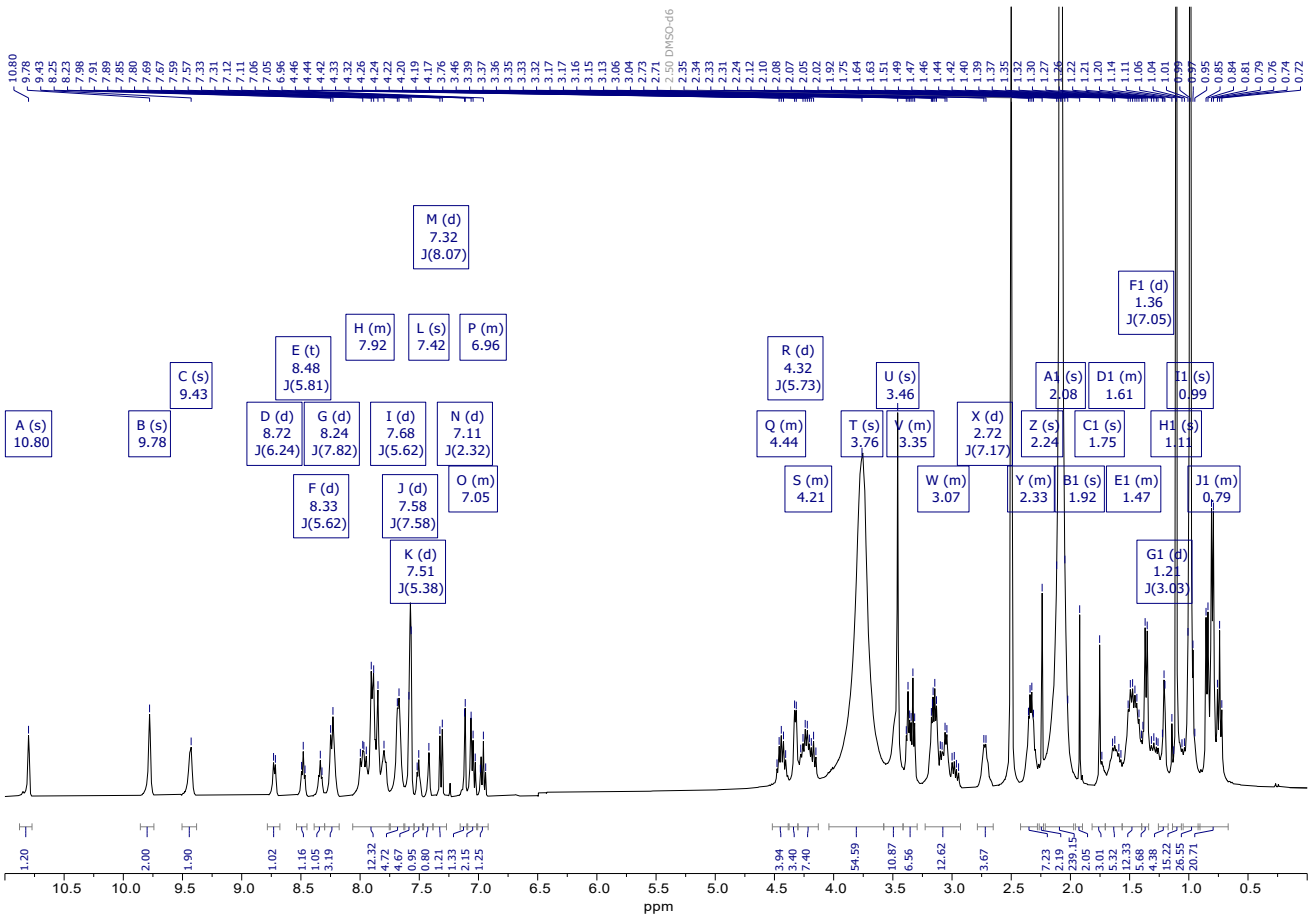

Figure S 18 - ^{1}H NMR spectrum of **C2$_{hom}$** measured in DMSO-d_6 at 400 MHz.

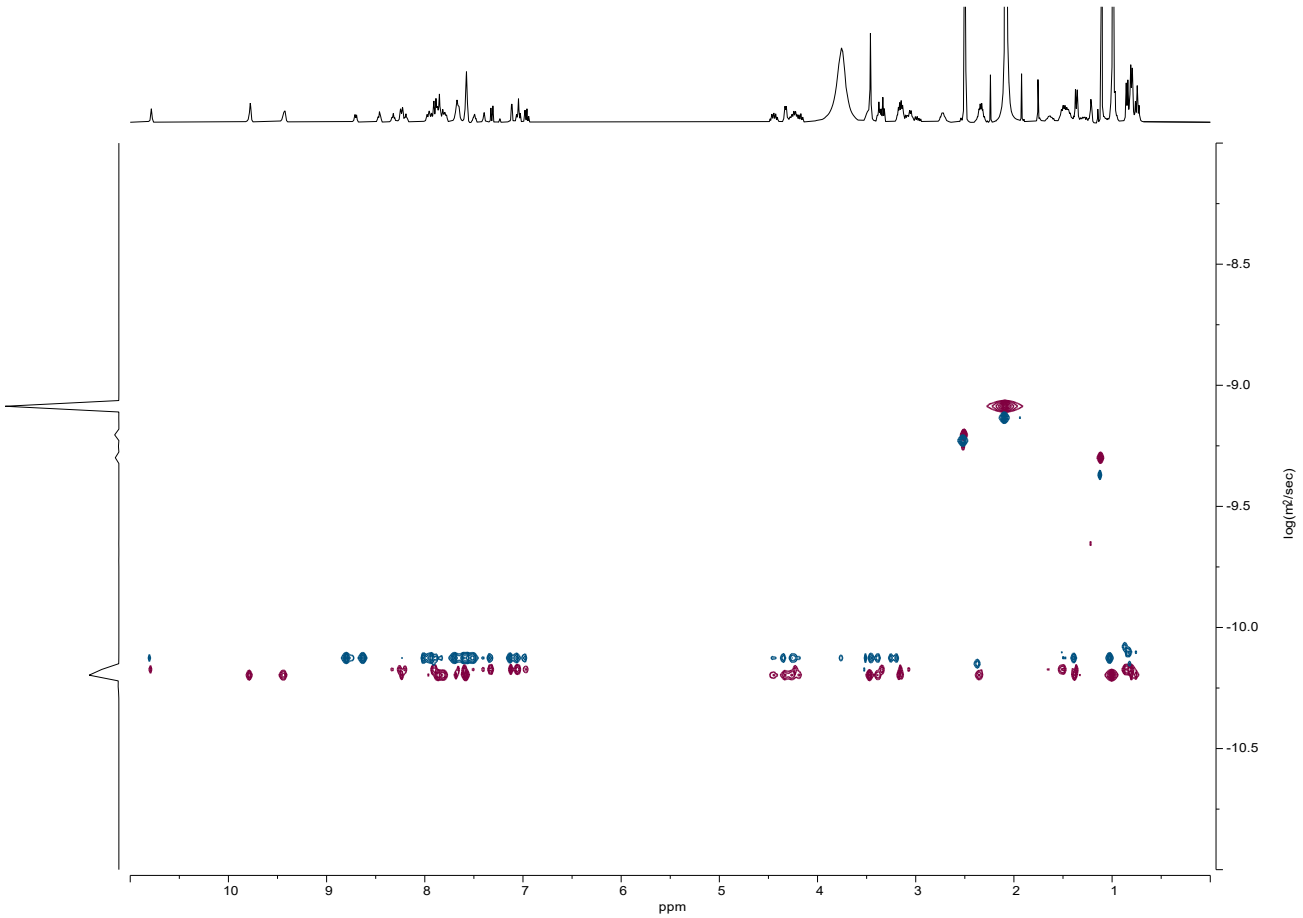

Figure S 19 - ^{1}H-DOSY NMR spectrum of **C2$_{hom}$** (purple) measured in DMSO-d_6 at 400 MHz. The ^{1}H-DOSY NMR spectrum of **L2** is shown in blue as reference.

2.3 Stability of $C1_{hom}$ and $C2_{hom}$ in DMSO (1 mM)

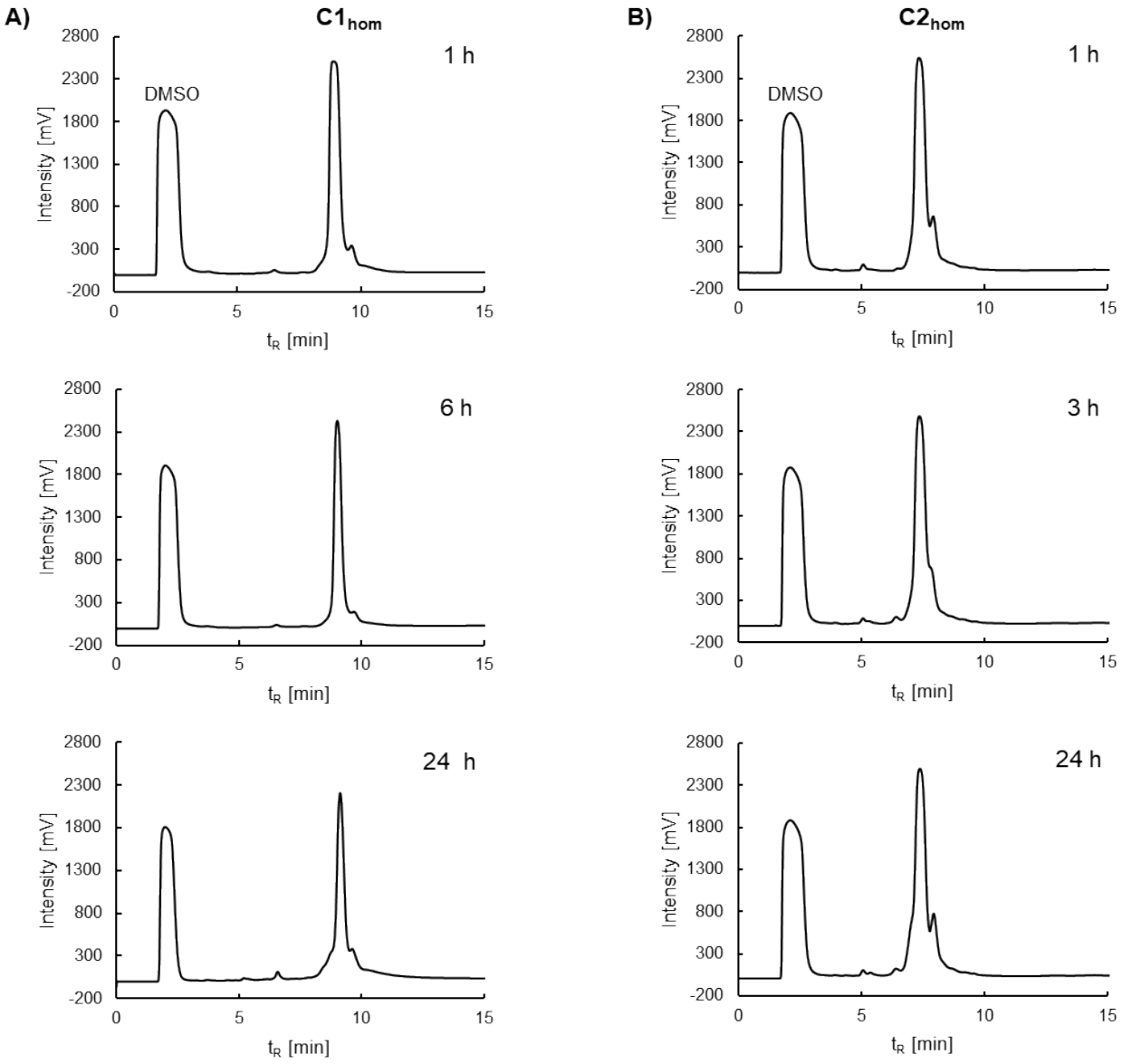

Figure S 20 - Stability of **$C1_{hom}$** (A) and **$C2_{hom}$** (B) after 1 h, 6 h/3 h and 24 h CDSA in DMSO at 1 mM concentration evaluated by RP-HPLC (40-70% B in 15min).

2.4 Stability of $C1_{hom}$ and $C2_{hom}$ in different solvents (0.1 mM)

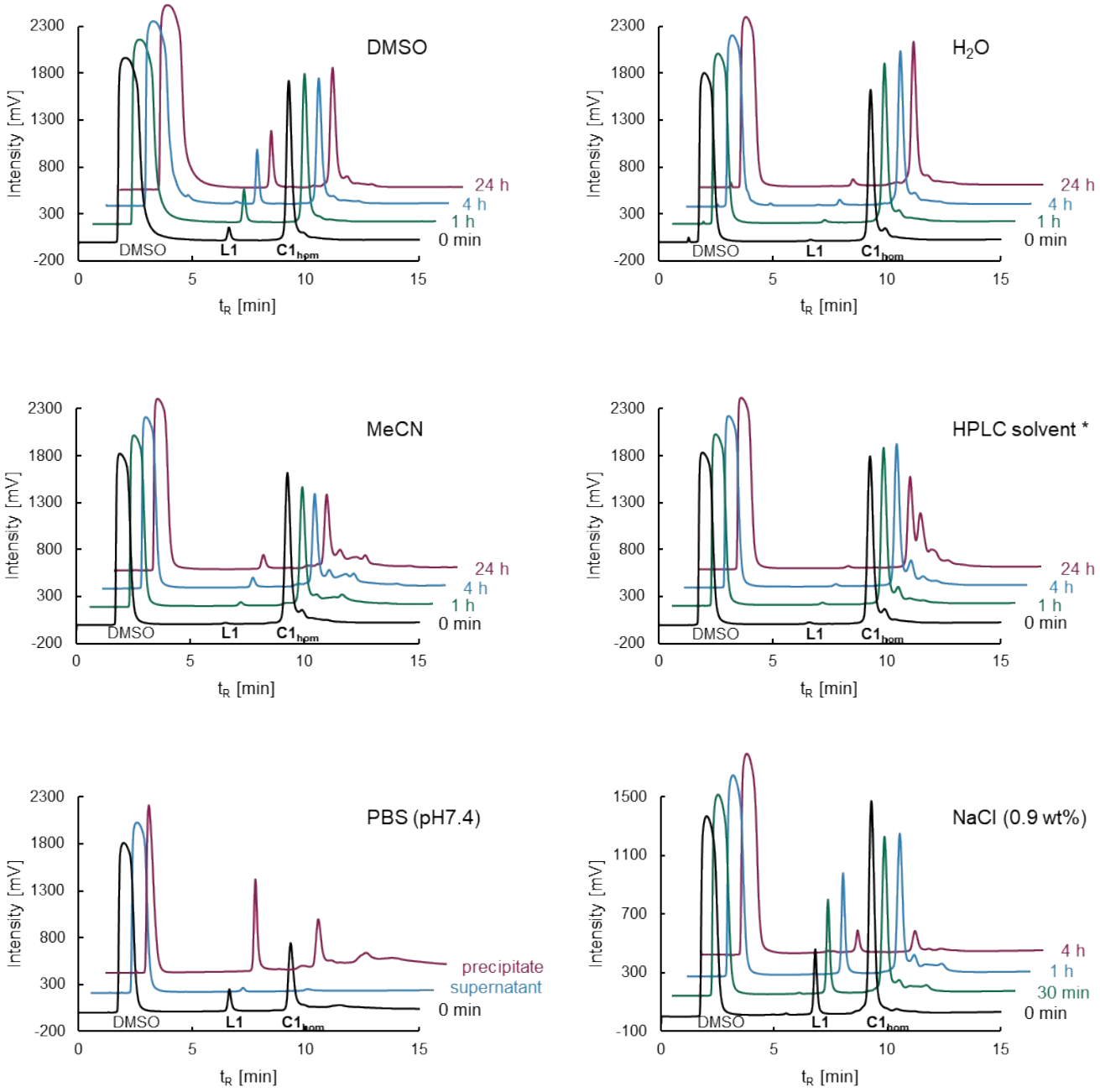

Figure S 21 - Stability of **$C1_{hom}$** (0.1 mM) in different solvents monitored by RP-HPLC (40-70% B in 15 min) up to 24 h. Precipitation occurred in salt containing solutions.

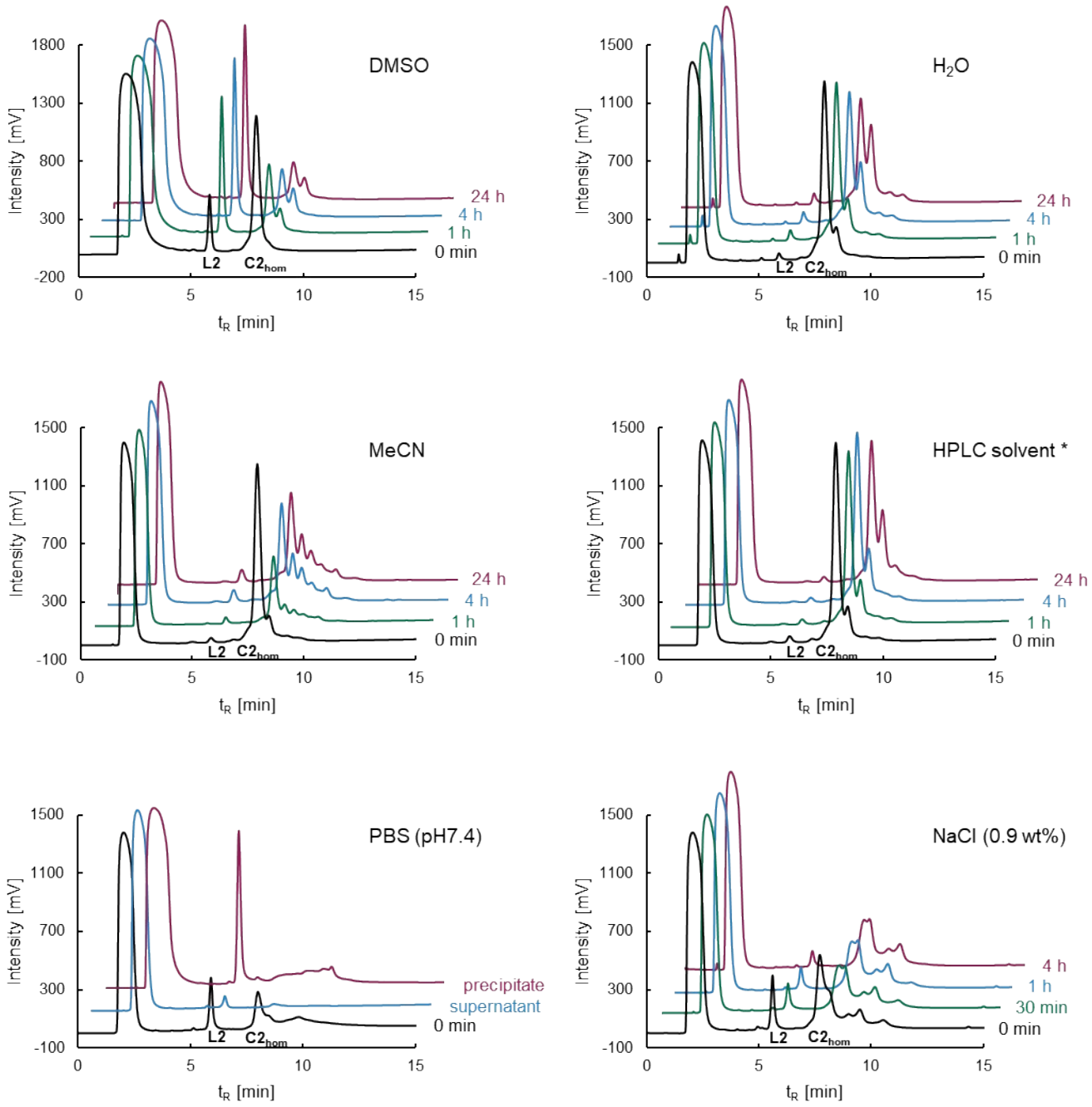

Figure S 22 - Stability of **$C2_{hom}$** (0.1 mM) in different solvents monitored by RP-HPLC (40-70% B in 15 min) up to 24 h. Precipitation occurred in salt containing solutions.

2.5 Concentration dependent formation of $C1_{hom}$ and $C2_{hom}$

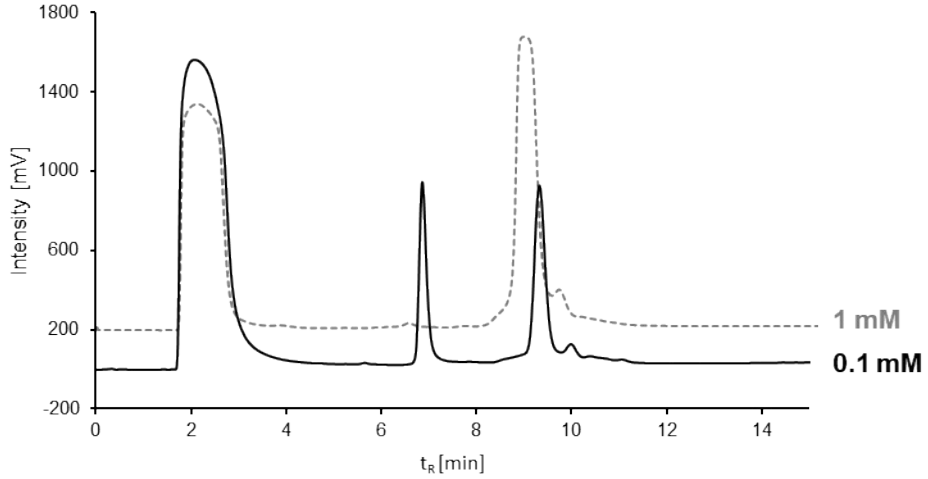

Figure S 23 - RP-HPLC chromatogram of **$C1_{hom}$** formed in a theoretical concentration of 0.1 mM in DMSO and measured with a gradient of 40-70% B in 15 min on a C18 column. As a reference the chromatogram of **$C1_{hom}$** in 1 mM concentration is depicted in a grey dashed line.

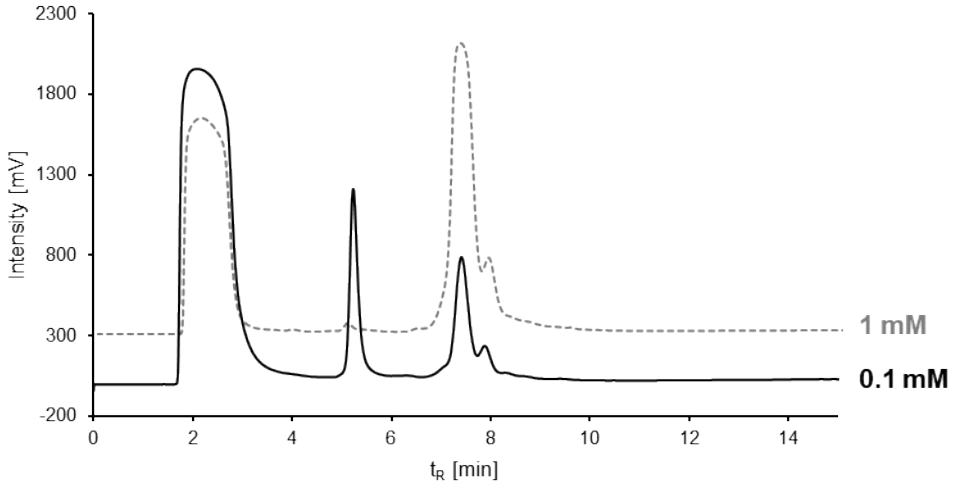

Figure S 24 - RP-HPLC chromatogram of **$C2_{hom}$** formed in a theoretical concentration of 0.1 mM in DMSO and measured with a gradient of 40-70% B in 15 min on a C18 column. As a reference the chromatogram of **$C2_{hom}$** in 1 mM concentration is depicted in a grey dashed line.

3 Heteroleptic metallacages $C1_{het}$ and $C2_{het}$

3.1 Characterization of $C1_{het}$

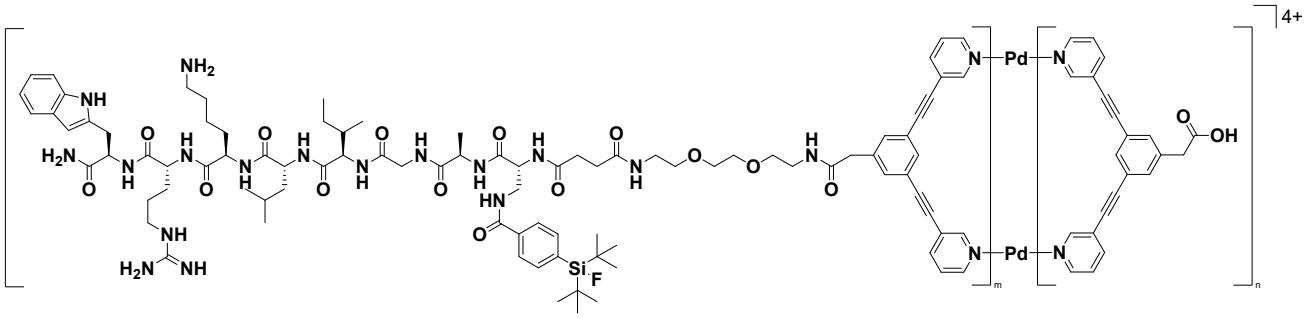

$[Pd_2(\mathbf{L1})(\mathbf{L0})_3]^{4+}$: m = 1, n = 3

$C_{156}H_{166}FN_{25}O_{20}Pd_2Si^{4+}$

2971.12 g/mol

$[Pd_2(\mathbf{L1})_2(\mathbf{L0})_2]^{4+}$: m = 2, n = 2

$C_{224}H_{276}F_2N_{42}O_{32}Pd_2Si_2^{4+}$

4375.94 g/mol

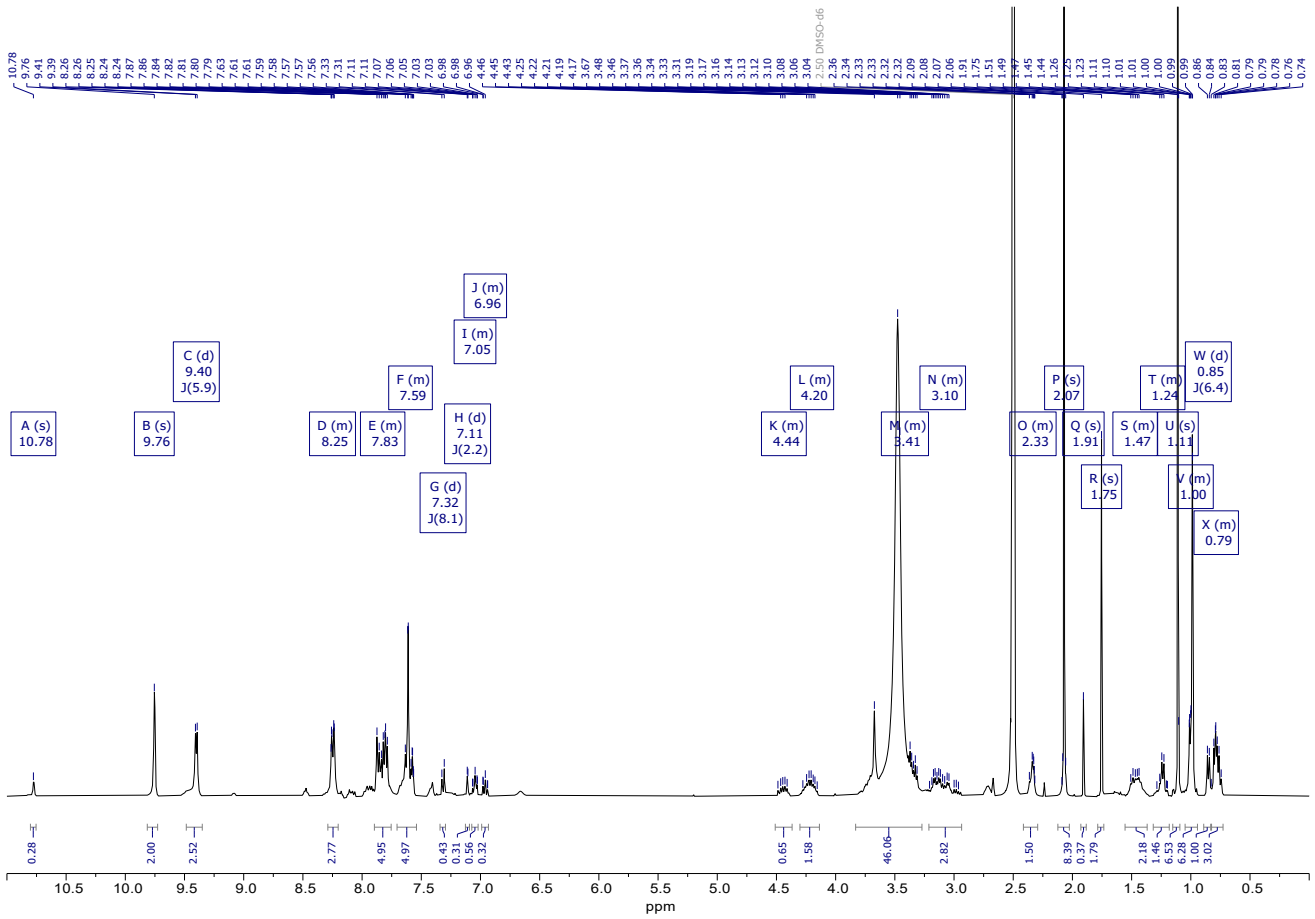

Figure S 25 - ^{1}H NMR spectrum of heteroleptic species obtained by the CDSA of **L1** (1.0 eq.) and **L0** (3.0 eq.) with $[Pd_2(MeCN)_4](BF_4)_2$ (2.0 eq.) measured in DMSO-d_6 at 400 MHz.

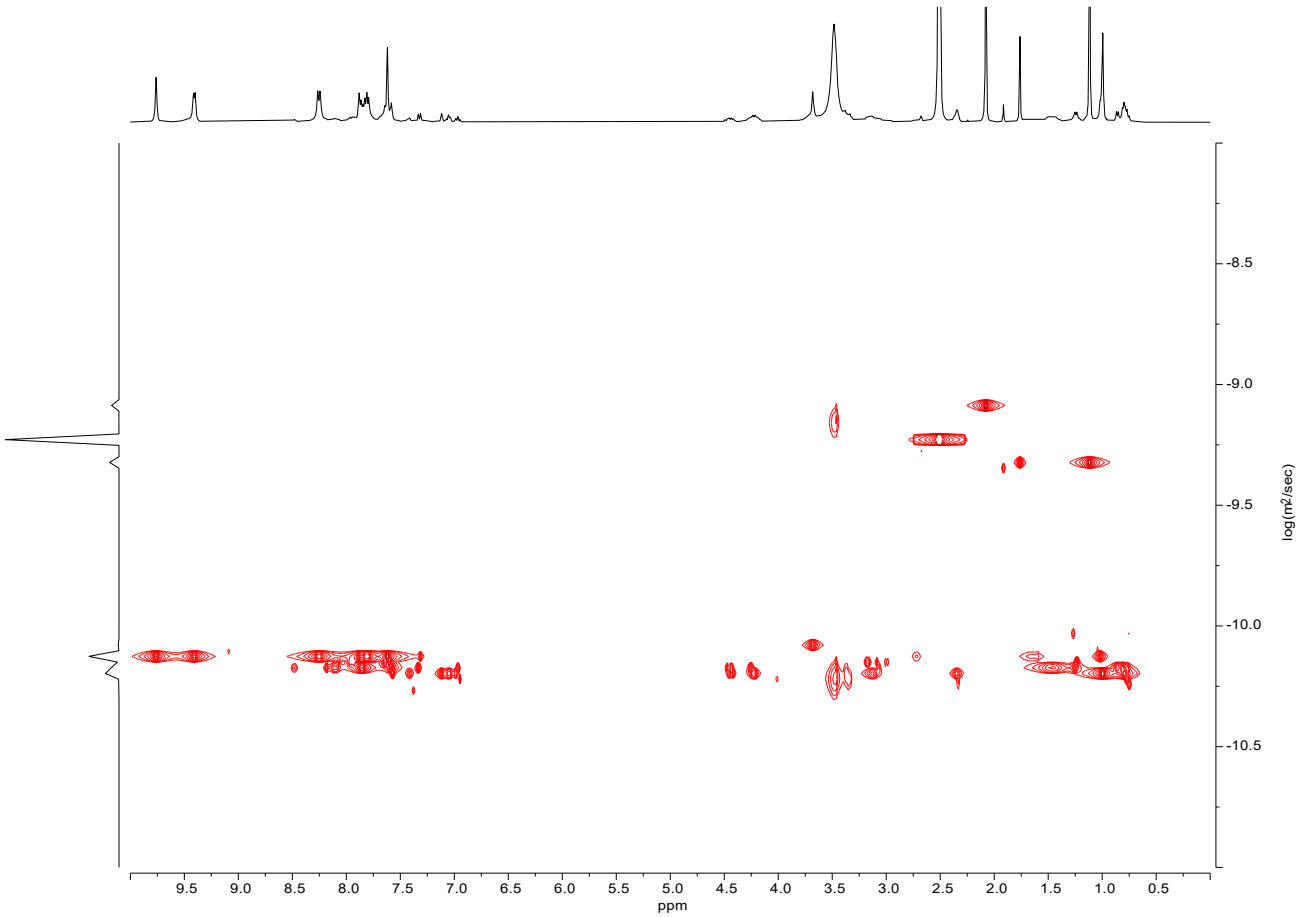

Figure S 26 - ^{1}H-DOSY NMR spectrum of heteroleptic species obtained by the CDSA of **L1** (1.0 eq.) and **L0** (3.0 eq.) with $[Pd_2(MeCN)_4](BF_4)_2$ (2.0 eq.) measured in DMSO-d_6 at 400 MHz.

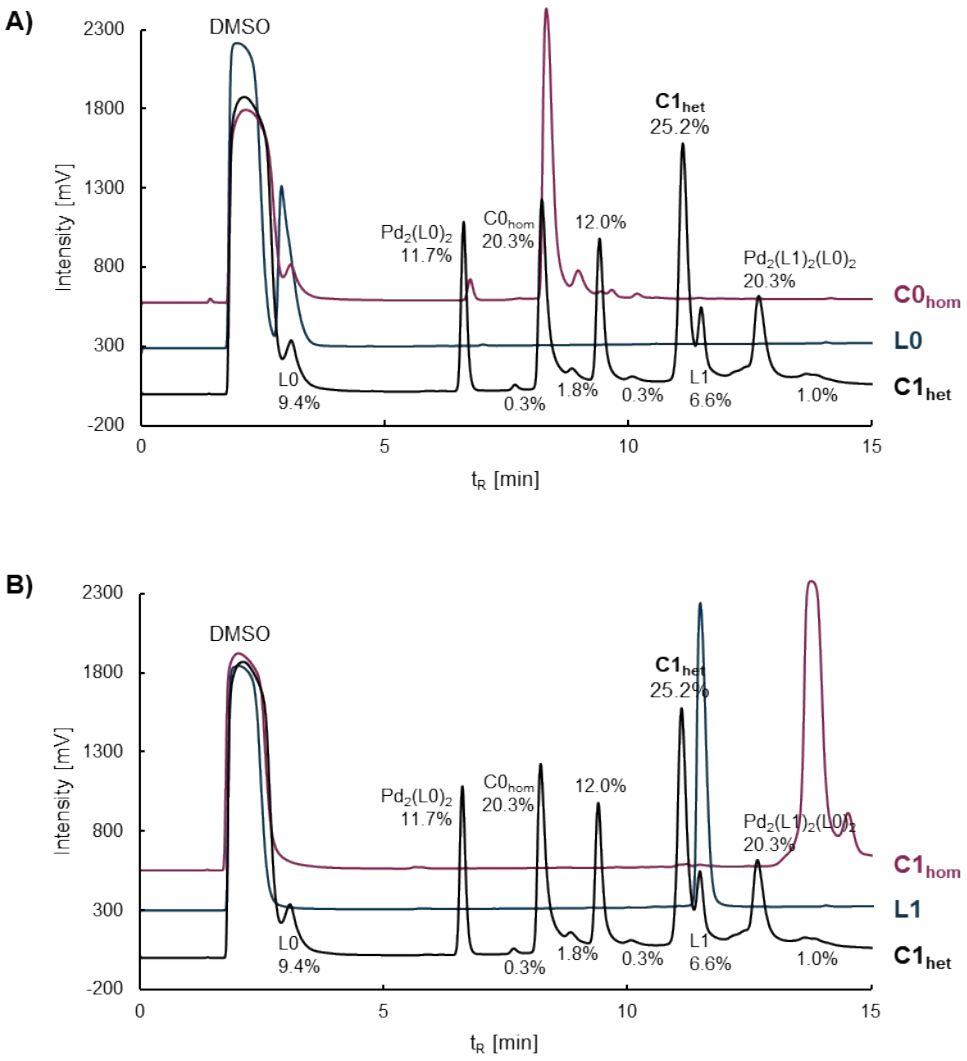

Figure S 27 - Comparison of the RP-HPLC chromatograms (30-60% B in 15 min, 1 mL/min) of heteroleptic species obtained by the CDSA of **L1** (1.0 eq.) and **L0** (3.0 eq.) with $[Pd_2(MeCN)_4](BF_4)_2$ (2.0 eq.) in DMSO. A) Comparison of the chromatogram with those of **L0** and **C0$_{hom}$**, and B) with those of **L1** and **C1$_{hom}$**.
t_R = 3.2 (L0), 6.6 (Pd_2L0_2), 8.3 ($C0_{hom}$), 9.4, 11.1 ($C1_{het}$), 11.5 (L1), 12.7 min ($Pd_2(L1)_2(L0)_2$).

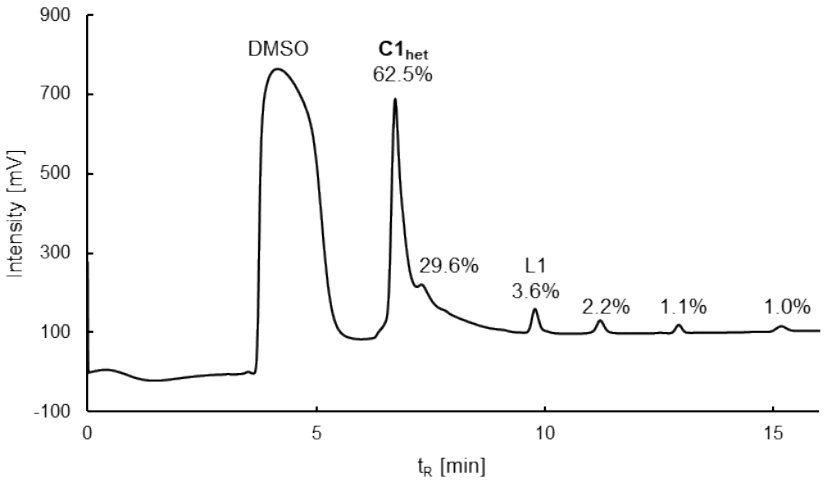

Figure S 28 - RP-HPLC chromatogram of heteroleptic species obtained by the CDSA of **L1** (1.0 eq.) and **L0** (3.0 eq.) with $[Pd_2(MeCN)_4](BF_4)_2$ (2.0 eq.) in DMSO using an optimized gradient: 20-40% B in 3 min, followed by 40-80% B in 15 min, 0.5 mL/min, 0.1% FA additive.

3.2 Characterization of $C2_{het}$

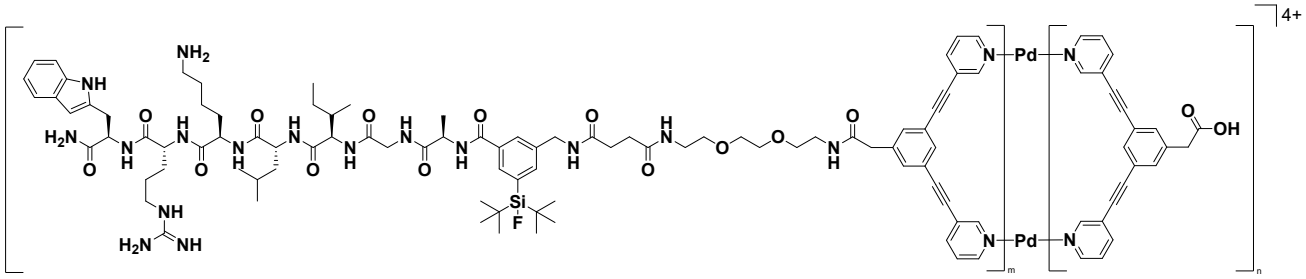

$[Pd_2(\mathbf{L2})(\mathbf{L0})_3]^{4+}$: m = 1, n = 3
$C_{154}H_{163}FN_{24}O_{19}Pd_2Si^{4+}$
2914.07 g/mol

$[Pd_2(\mathbf{L2})_2(\mathbf{L0})_2]^{4+}$: m = 2, n = 2
$C_{220}H_{270}F_2N_{40}O_{30}Pd_2Si_2^{4+}$
4261.83 g/mol

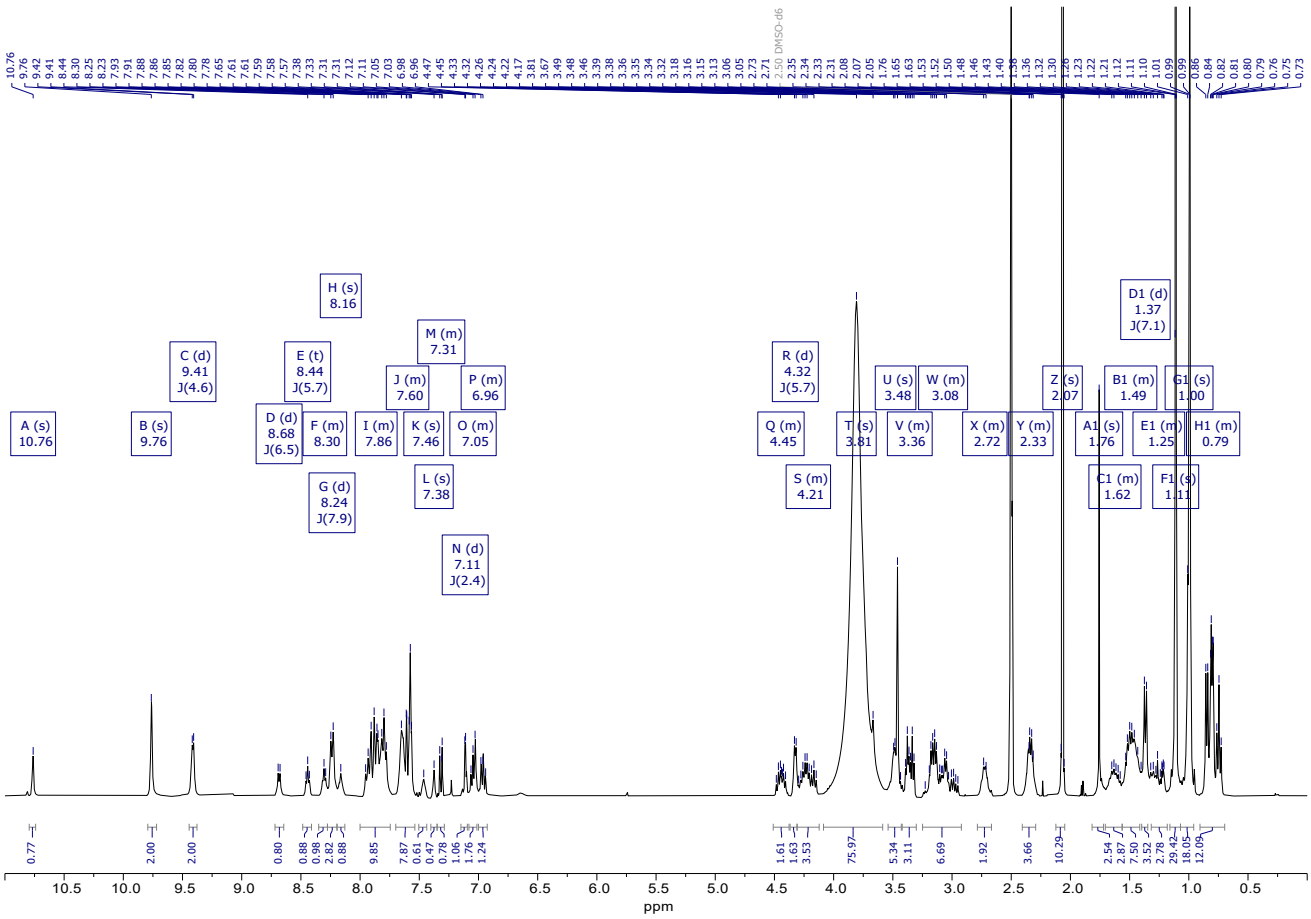

Figure S 29 - ^{1}H NMR spectrum of heteroleptic species obtained by the CDSA of **L2** (2.7 eq.) and **L0** (1.3 eq.) with $[Pd_2(MeCN)_4](BF_4)_2$ (2.0 eq.) measured in DMSO-d_6 at 400 MHz.

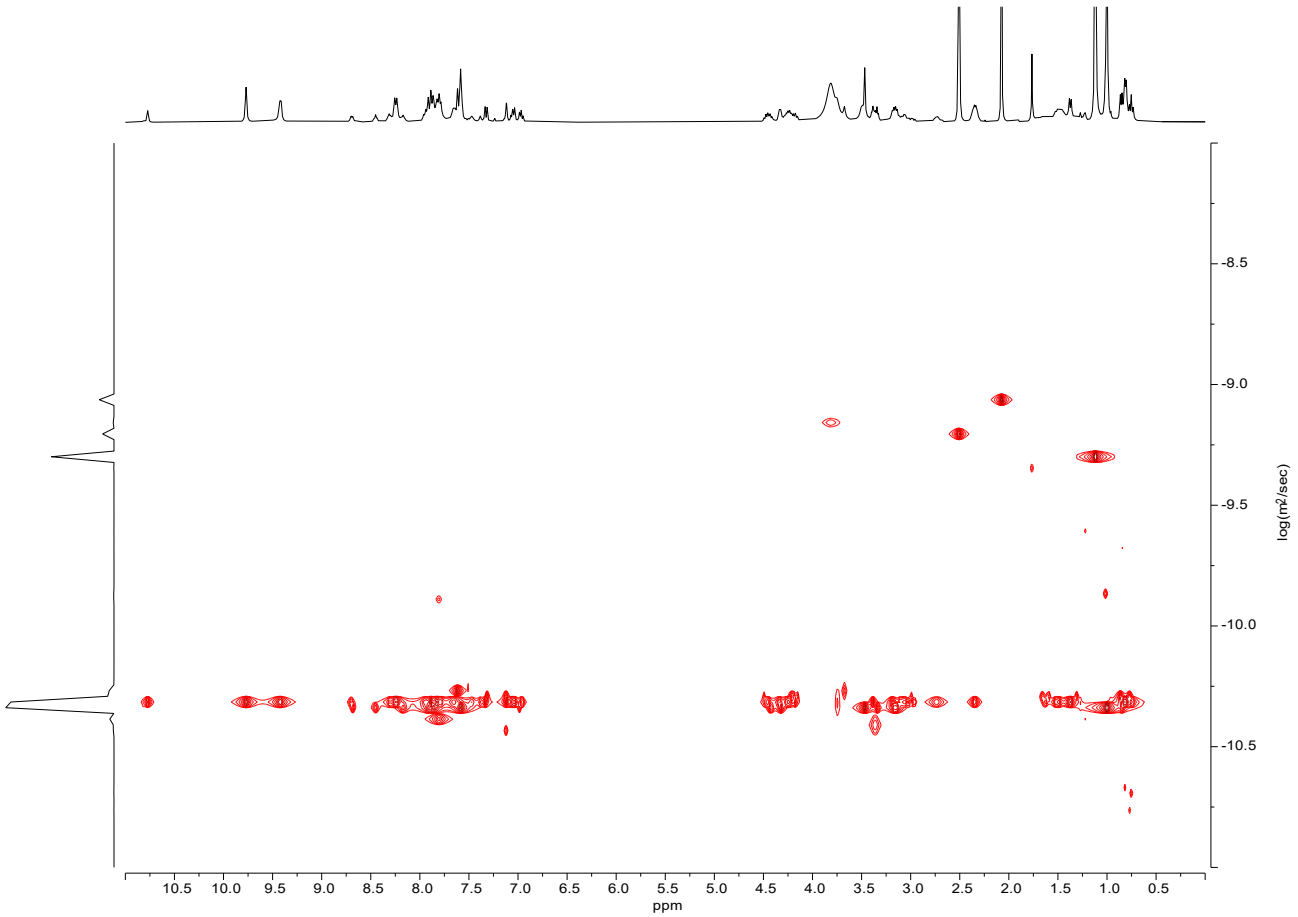

Figure S 30 - ^{1}H NMR spectrum of heteroleptic species obtained by the CDSA of **L2** (2.7 eq.) and **L0** (1.3 eq.) with $[Pd_2(MeCN)_4](BF_4)_2$ (2.0 eq.) measured in DMSO-d_6 at 400 MHz.

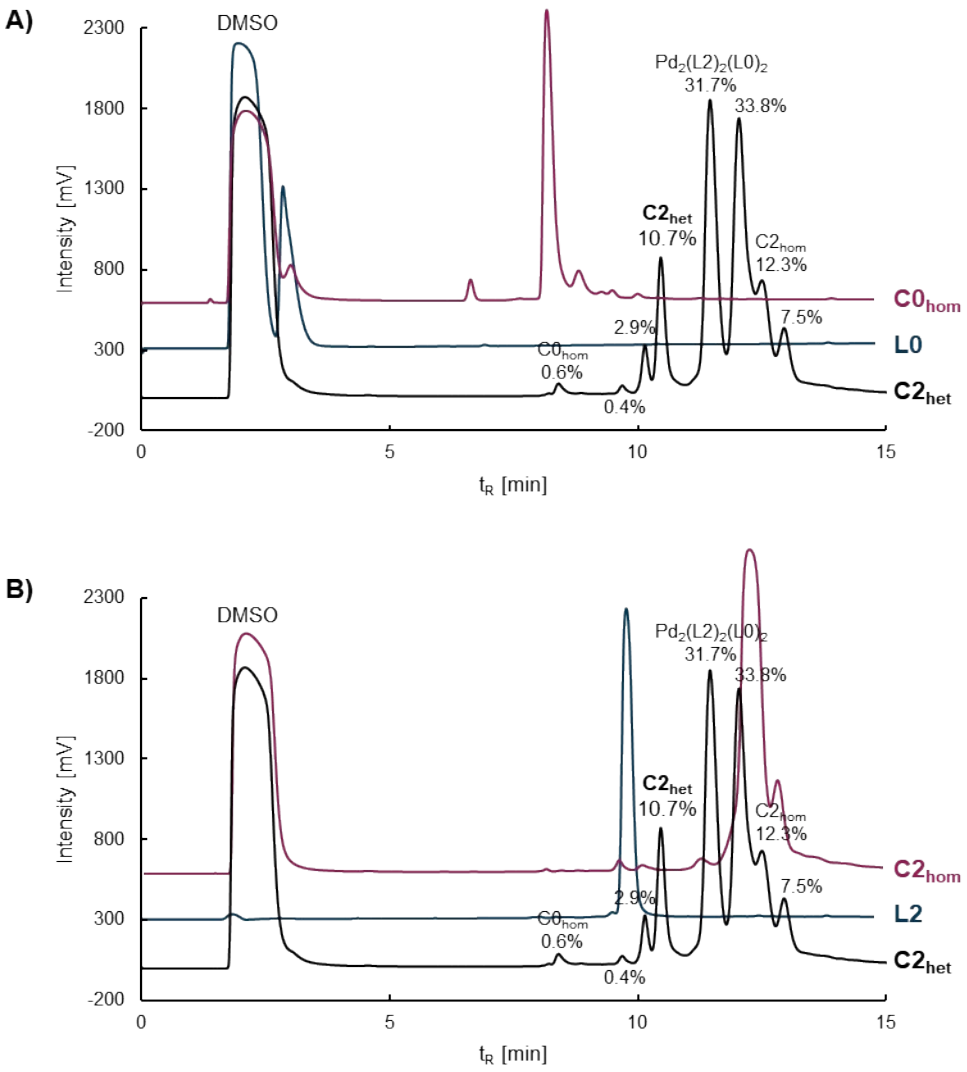

Figure S 31 - Comparison of the RP-HPLC chromatograms (30-60% B in 15 min, 1 mL/min) of heteroleptic species obtained by the CDSA of **L2** (2.7 eq.) and **L0** (1.3 eq.) with $[Pd_2(MeCN)_4](BF_4)_2$ (2.0 eq.) in DMSO. A) Comparison of the chromatogram with those of **L0** and **$C0_{hom}$**, and B) with those of **L2** and **$C2_{hom}$**.
t_R = 10.2, 10.5 ($C2_{het}$), 11.5 ($Pd_2(L2)_2(L0)_2$), 12.1, 12.6 ($C2_{hom}$), 13.0 min.

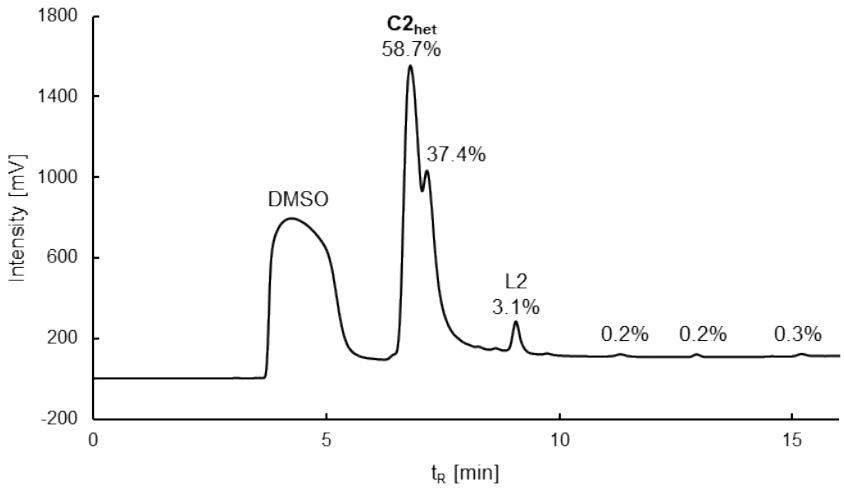

Figure S 32 - RP-HPLC chromatogram of heteroleptic species obtained by the CDSA of **L2** (2.7 eq.) and **L0** (1.3 eq.) with $[Pd_2(MeCN)_4](BF_4)_2$ (2.0 eq.) in DMSO using an optimized gradient: 20-40% B in 3 min, followed by 40-80% B in 15 min, 0.5 mL/min, 0.1% FA additive.

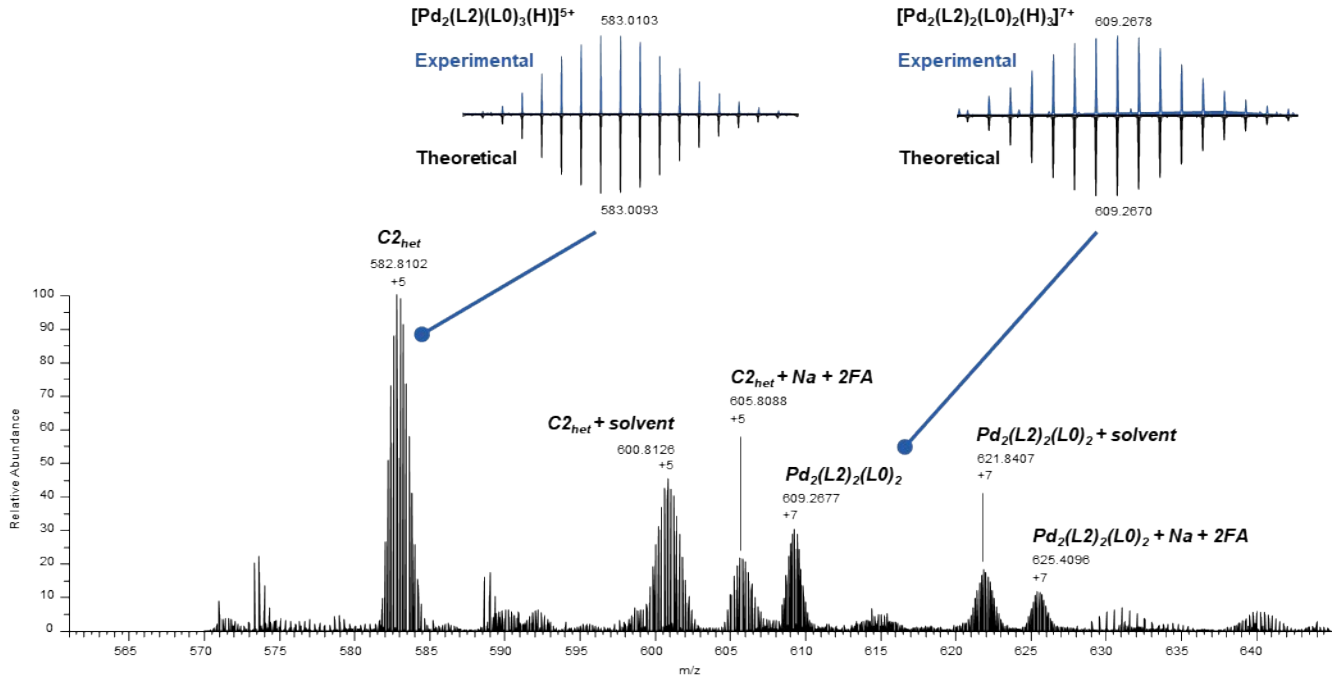

Figure S 33 - DI-HR-ESI-MS of heteroleptic species obtained by the CDSA of **L2** (2.7 eq.) and **L0** (1.3 eq.) with $[Pd_2(MeCN)_4](BF_4)_2$ (2.0 eq.) in DMSO.

4 Encapsulation of ReO_4^-

$C1_{hom}$

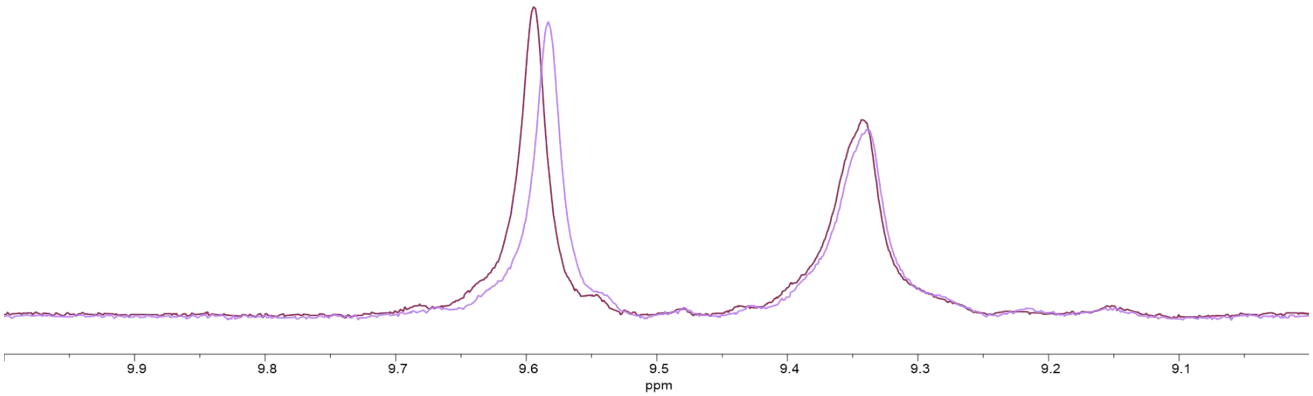

Figure S 34 - Superimposed ^{1}H NMR spectra of **$C1_{hom}$** (dark purple) and **$C1_{hom}$** + 2 eq. $NaReO_4$, incubated for 30 min (light purple). The spectra were recorded in DMSO-d_6/D_2O (1/1) at 400 MHz.

$C2_{hom}$

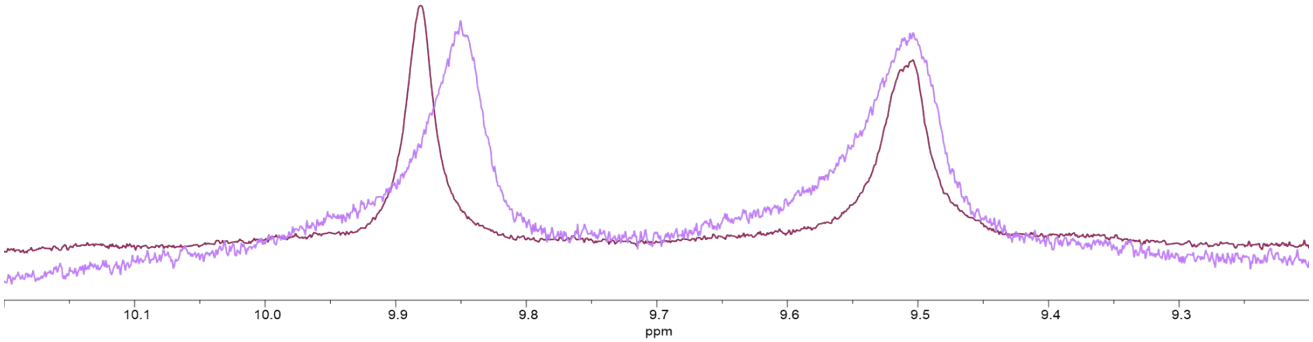

Figure S 35 - Superimposed ^{1}H NMR spectra of **$C2_{hom}$** (dark purple) and **$C2_{hom}$** + 2 eq. $NaReO_4$, incubated for 30 min (light purple). The spectra were recorded in DMSO-d_6/D_2O (1/1) at 400 MHz.

5 Characterization of radiolabeled ligands

5.1 ^{18}F-L1

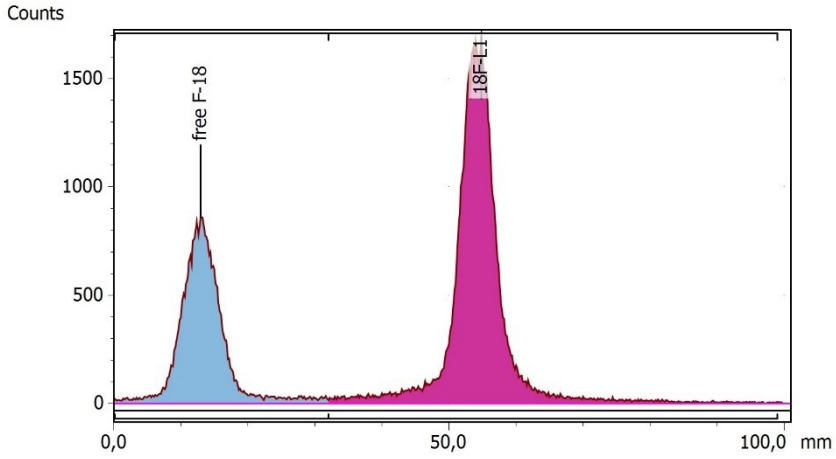

Figure S 36 - reaction control of **^{18}F-L1** via radio TLC using MeCN/H_2O, 8/2, +10% sodium acetate (2 M), +1% TFA as the solvent system.

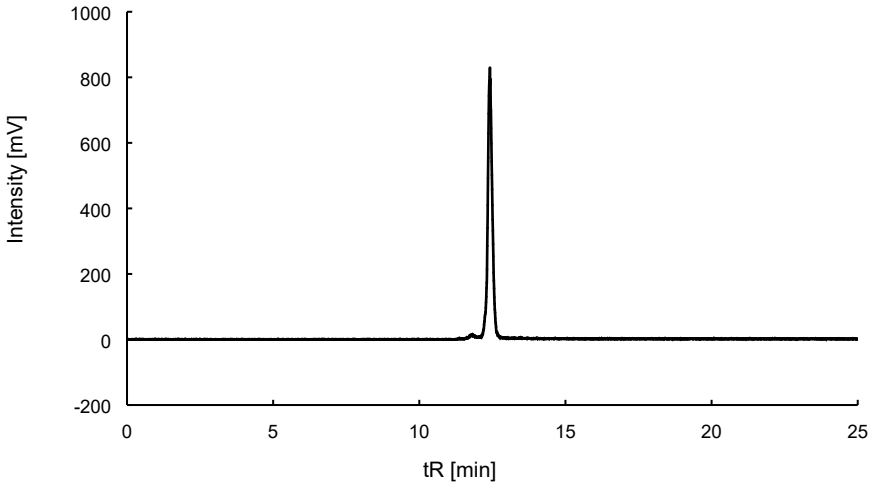

Figure S 37 - radio-RP-HPLC chromatogram of **^{18}F-L1** measured with a gradient of 10-80% B in 15 min on a C18 column.

5.2 ^{18}F-L2

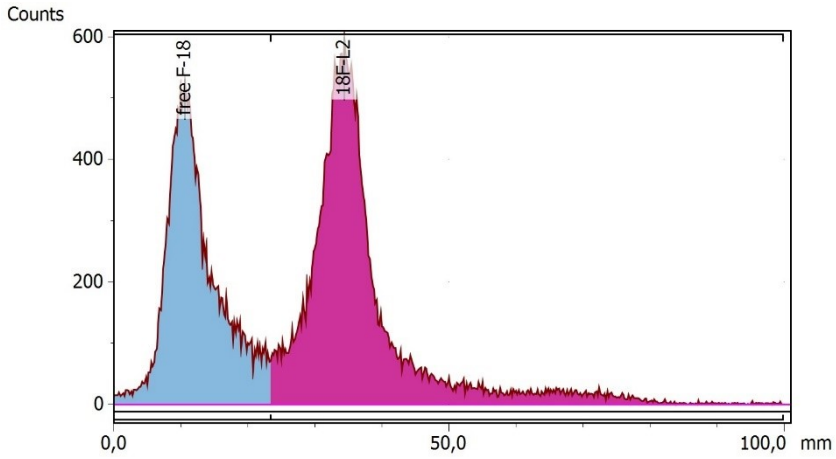

Figure S 38 - reaction control of **^{18}F-L2** via radio TLC using MeCN/H_2O, 8/2, +10% sodium acetate (2 M), +1% TFA as the solvent system.

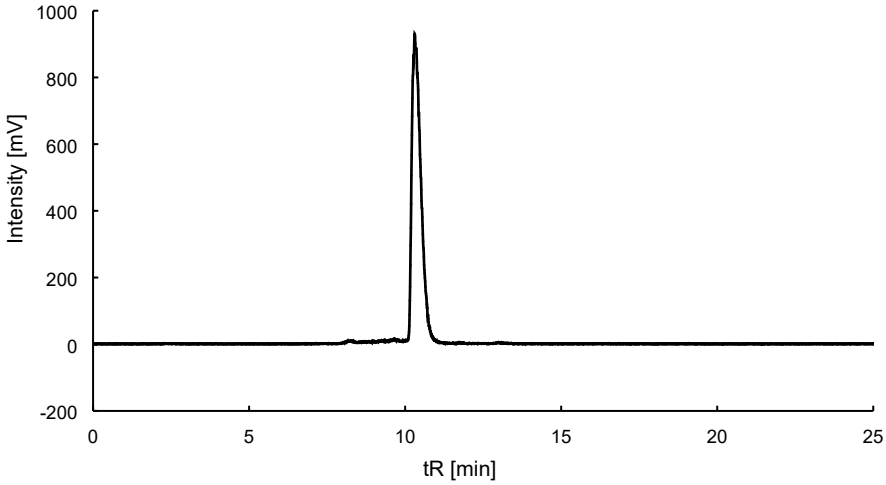

Figure S 39 - radio-RP-HPLC chromatogram of **^{18}F-L2** measured with a gradient of 10-80% B in 15 min on a C18 column.

6 Literature examples of Pd-based metallacages for imaging applications

Table S 1 - Lantern-shape MCgs of the $Pd_2L_4^{n+}$ family developed for imaging applications (fluorescence or nuclear imaging) and respective limitations.

***Exo*-Functionalization**	**Imaging application**	**Limitations**	**Reference**
Ru(bipy) via Click Chemistry	Fluorescence imaging	Non targeted cage.	Elliott et al. 2016 DOI: 10.1021/acs.inorgchem.5b02843
Naphtyl, anthracenyl via amide coupling	Fluorescence imaging	Non targeted cage.	Schmidt et al. 2016 DOI: 10.1039/c6dt00654j
Ru(bipy), Ru(terpy) via amide coupling	Fluorescence imaging	Non targeted cage.	Schmidt et al. 2016 DOI: 10.1039/c6dt02708c
BODIPY via amide coupling/Click chemistry	Fluorescence imaging	Instability towards GSH and PBS (pH 7.4). Non targeted cage.	Woods et al. 2019 DOI: 10.1016/j.jinorgbio.2019.110781
BBB targeting peptide	SPECT imaging via $^{99m}TcO_4^-$ encapsulation	Instability of the host-guest complex towards GSH, moderate stability *in vivo.*	Woods et al. 2021 DOI: 10.1021/acs.bioconjchem.0c00659
BODIPY via amide coupling	Fluorescence imaging	Non targeted cage.	Aikman et al. 2022 DOI: 10.1039/d2dt00337f
^{18}F-AMBF$_3$ via Click Chemistry	PET imaging and drug delivery (via encapsulation)	Instability of the host-guest complex *in vivo.* Non targeted cage.	Cosialls et al. 2023 DOI: 10.1002/chem.202202604
^{177}Lu-DOTA-TATE*	SPECT imaging and β^- therapy	Increased lipophilicity, instability towards PBS, HBSS and cell culture medium, competition of radiometal with Pd(II)	Deiser et al. 2023 DOI: 10.1021/acs.inorgchem.3c02090

* In this case, a heteroleptic MCg was obtained.